1-1-2005

Field testing and finite element analysis of retrofit methods for distortion-induced fatigue in steel bridges

Yared Shifferaw Bayleyegn
Iowa State University

Field testing and finite element analysis of retrofit methods for distortion-induced fatigue in steel bridges

by

Yared Shifferaw Bayleyegn

A thesis submitted to the graduate faculty

in partial fulfillment of the requirements for the degree of

MASTER OF SCIENCE

Major: Civil Engineering (Structural Engineering)

Program of Study Committee:
Fouad S. Fanous (Major Professor)
Terry J. Wipf
Lester W. Schmerr

Iowa State University

Ames, Iowa

2005

Graduate College

Iowa State University

This is to certify that the master's thesis of

Yared Shifferaw Bayleyegn

has met the thesis requirements of Iowa State University

Signatures have been redacted for privacy

TABLE OF CONTENTS

LIST OF FIGURES

LIST OF TABLES

ACKNOWLEDGEMENTS

Praise to the Almighty through whom everything has been possible. I would like to express my ineffable gratitude to all those who have contributed to this fruition. My father, Shifferaw Bayleyegn, takes all the credit for instilling the love of education inside me, and my mother, Yimegnushal Demilie, for all the unconditional love she has showered me with all my life. May God bless Dr. Fouad Fanous, my major professor, for the guidance and invaluable advice in the course of this work. My heartfelt appreciation also goes to the Ethiopian community in Ames, Iowa, who has given me moral support and made me feel at home: Abdulmalik Shiffa and his wife Leila, Dr. Abebe Hassen and his wife Meseret, Dr. Girma Melese and his wife Helen, and Wolette Ammanuel.

ABSTRACT

Crack formation due to out-of-plane distortion in the web-gap region has been a common occurrence in multi-girder steel bridges. These cracks result from the fatigue stresses that are induced in the web-gap due to cyclic diaphragm forces resulting from differential deflections between girders. The study presented herein investigated the different repair methods that can be used to control formation of these cracks.

The study involved field testing and analytical modeling of a skewed multi-girder steel bridge designated as Design No.1283, which is built on county road D-180 that crosses over I-380 in the state of Iowa. Different repair methods were suggested to reduce the induced stresses and strains in the web-gap under truck loads. These methods included loosening of the bolts connecting the cross-bracing to the stiffener, connecting the stiffener to the girder top flange or adding another stiffener on the opposite side of the girder web. The results indicated that the first two of these repair alternatives were effective in reducing induced stresses and strains in the web-gap region.

The impact of web-gap height on the distortion induced in the web-gap was also studied. Furthermore, influence surfaces for different

responses such as, web-gap strains, stresses, out-of-plane displacements at critical locations, and forces in the adjacent diaphragm were developed. Moreover, relationships between the relative out-of-plane displacements and vertical stresses induced within the web-gap region were also provided. These developed relationships and surfaces serve as a quick estimate of induced stresses at critical locations in other web-gap regions of the bridge.

1. INTRODUCTION

1.1 Introduction

According to published literature, the number of deficient bridges on the nation's highway system is increasing. Crack formation due to fatigue stress is among the factors that cause damage to bridge structures. For example, in a multi-girder steel bridge where diaphragms are used, cracks have been seen to be formed in an area that is referred to, among bridge engineers, as web-gap. This is the region between the diaphragm-stiffener fillet weld and the flange which has been left un-stiffened (See Fig.1.1). Until recent years, the specifications of the American Association of State and Highway Transportation Officials (AASHTO) did not allow designers to connect or weld web-stiffeners to the tension flanges of steel girders.

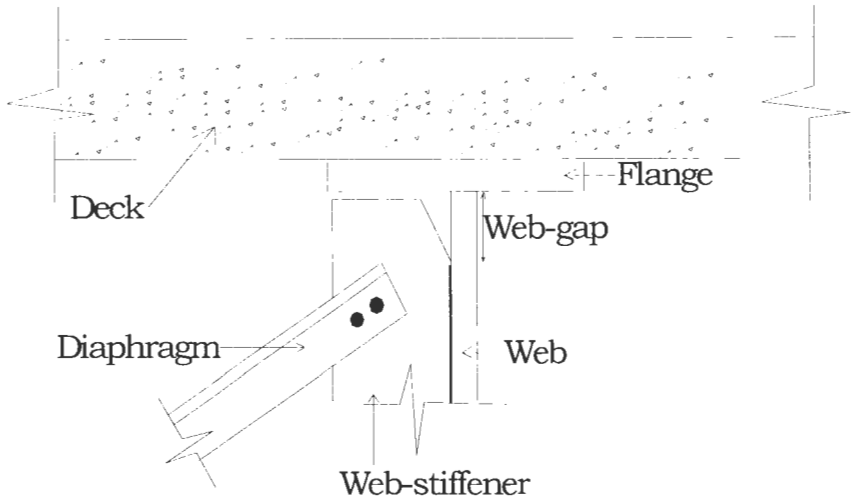

Figure 1.1 Schematic of web-gap with no-retrofit

Engineers and researchers believe that out-of-plane distortion remains to be the main cause of crack formation in the web-gap region. This distortion is the result of the differential deflection between two adjacent girders that are connected by diaphragms. As traffic passes on a bridge, differential deflections occur among adjacent girders. The relative deflections of these girders induce forces in the diaphragms that are then transferred to the web gap through the connections between the diaphragms and web-stiffeners. These forces result in bending of the web-gap and therefore induce stresses in the vertical direction that yield to the formation of horizontal cracks. In a multi-girder bridge, especially with high average daily traffic, periodic loading induces stresses that will result in reducing the fatigue life of the bridge.

Within the past few years, several researches have been conducted to account for alternatives to mitigate existing crack propagation or to prevent cracks from initiating in the web-gap regions of multi-girder steel bridges. As many bridges elsewhere in the United States, it has been found that several of the multi-girder steel bridges in the State of Iowa experience the type of problem discussed above. Recently, researchers at Iowa State University have also conducted several studies to investigate the cause and methods of retrofitting or preventing the formation of cracks in the web-gap region of several steel bridges in Iowa. The study presented herein

complements these works by conducting experimental and analytical investigation on a multi-girder steel bridge, the objectives of which are detailed in the next section.

This chapter describes the objective and scope of the study on web-gap deformation of a multi-girder steel bridge. A literature review of related works done by other researchers with respect to web-gap distortion is also presented.

1.2 Objective and scope

The objectives of the study presented herein have been to investigate experimentally and analytically the behavior of the web-gap in a multi-girder steel bridge subjected to out-of-plane distortion and recommend retrofit alternatives to reduce or prevent formation of cracks in such region.

These objectives were accomplished by conducting field tests on the multi-girder steel bridge and developing a finite element model of the structure for analysis. The analytical results from the finite element were compared with field test results of the bridge to verify the suitability of the analytical modeling.

The developed finite element model was used to investigate the general behavior of the web-gap in the multi-steel girder bridge. The impact of load positioning on induced web-gap distortion was investigated for different loading cases applied on the finite element model. The results of the finite element analyses for these cases were compared with corresponding field test results and the appropriateness of the model in predicting the web-gap distortion phenomenon was verified.

Several retrofit methods that included loosening of bolts connecting diaphragm members to the vertical stiffeners, connecting the vertical stiffener to the flange of the girder and utilizing additional stiffeners on the outer side of the exterior girder were investigated (See Fig.1.2). Also, the effect in web-gap deformation behavior with respect to web-gap height variation was studied.

To understand the distortion within the web-gap region influence surfaces for different responses were developed using a unit load (1kip) applied at various locations on the bridge model. Influence surfaces were developed for vertical strain, out-of-plane displacement at the test and other critical locations in the web-gap region, as well as the force in the adjacent diaphragm member.

The influence surfaces for strains would provide quick estimate of the strains that develop in the web-gap region as loads move across the multi-girder steel bridge. This would aid the bridge engineer to determine the effect of truck load positions on the strains induced in the web-gap region. The influence surfaces for the resultant force in the diaphragm and out-of-plane relative displacement at the critical locations of the web-gap were developed to understand the correlation between diaphragm force, out-of-plane relative displacement and induced strains in the web-gap region. In addition, relationships between vertical stress and relative out-of-plane displacement were established that would aid in a quick prediction of web-gap stress based on field out-of-plane measurements.

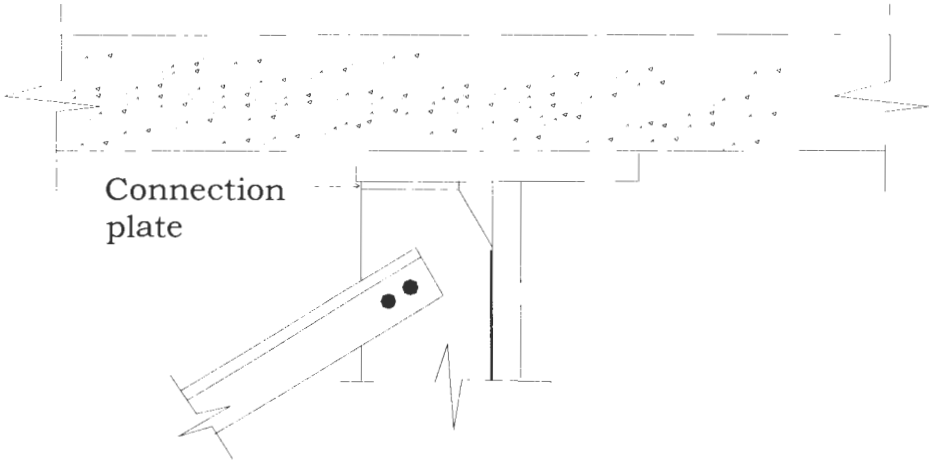

a. As-built - retrofit with connection plate (Retrofit A)

Figure 1.2 Schematic of web-gap with different alternative retrofits

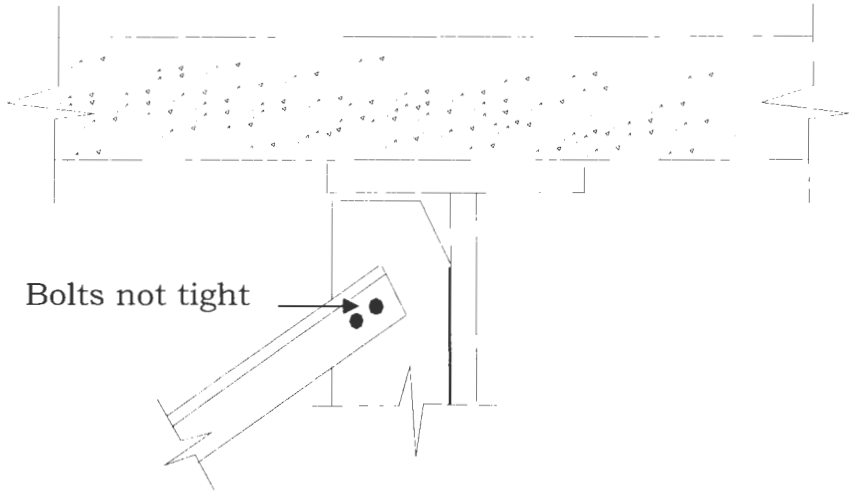

b. Full-bolt loosening retrofit (Retrofit B)

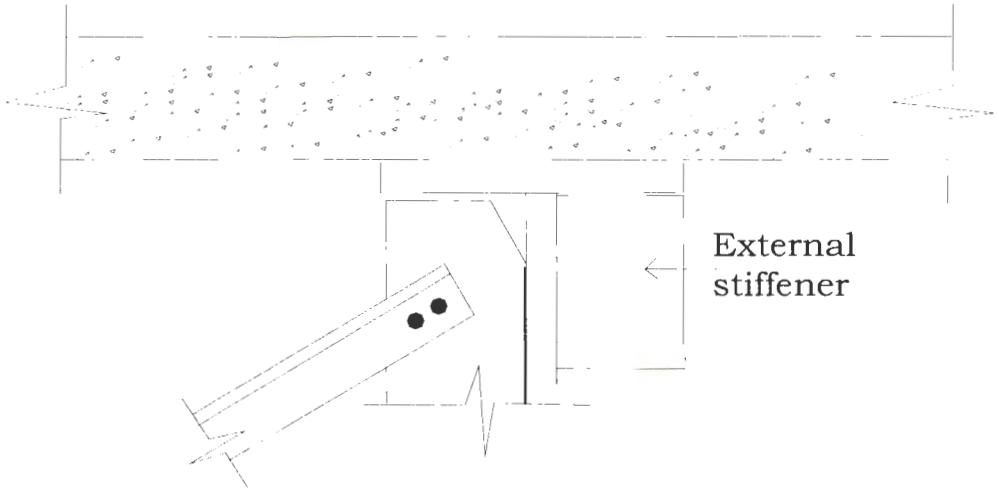

c. External stiffener retrofit (Retrofit C)

Figure 1.2 (Cont.)

1.3 Literature review

In 1989, experimental research on the causes and possible retrofit techniques for distortion-induced cracking of steel girder bridges at web-gap regions was performed by Fisher, et al. as cited in [8]. The results showed that using k-type rather than utilizing x-type diaphragms in steel girder bridges where web-gap exists resulted in a longer fatigue life. The following were some of the retrofit methods and related findings suggested by Fisher and his colleagues.

- Providing positive attachment by welding or bolting the stiffener to the top flange was found to be the most effective. However, this method has limitations since traffic should be interrupted during welding and the difficulty of achieving high-quality welds.
- Drilling holes at the crack tip to prevent further crack propagation would be satisfactory if the crack had propagated into a lower stress region.

The effect of removal of the diaphragms from steel bridges to eliminate fatigue cracking caused by diaphragm forces was investigated by Cousins, et al.(cited in [8]). Tests were conducted on a three-span multiple girder bridges to establish the magnitude of load distribution done by diaphragms based on a load distribution factors. The results showed that only 5% to 15% strain difference resulted with the diaphragm removal. Cousins and

his colleagues concluded that this difference was insignificant to offset the load rating of a bridge structure. They recommended removing the unnecessary diaphragms that are not required for load distribution or stability. Similar recommendations were also proposed by Keating (cited in [8]). Moreover, Azizinamini, et al. (cited in [9]) studied the lateral torsional stability of multiple steel girder bridges which ensues diaphragm removal. Using the AASHTO design manual Azizinamini, et al., as cited in [9], showed that no instability would occur following diaphragm removal.

The Iowa Department of Transportation (Iowa DOT) in collaboration with Iowa State University's Centre for Transportation Research and Education (CTRE) and the Bridge Engineering Centre (BEC), conducted several field studies on different bridges to investigate cracking in the web-gap region. In the 1980's, the researchers recommended drilling holes to terminate the propagation of cracks [9]. However, this retrofit method was found to be ineffective due to the high stresses that could not be any further contained with the drilling terminus. Since the 1990's, loosening of bolts connecting the diaphragms with the web-stiffeners has been used by Iowa DOT. Wipf, et. al. [9] have found that this approach was effective in reducing the impact of the force that is created as a result of differential deflection of between the girders and hence resulting reducing the bending stress in the web-gap region.

In 1998, Khalil, et al. [4] experimentally investigated the cracking problems occurring at the diaphragm and girder connections in negative moment regions of continuous plate girder bridges. Bolt-loosening at the diaphragm -stiffener connection was utilized by Khalil, et al. [4] as a crack prevention method. Comparison of out-of-plane distortions of the web for x- and k-type diaphragms of skewed and non-skewed bridges was made. The following were some of the findings reported by Khalil, et al. [4]:

- Comparison of stress ranges in web gaps with loose diaphragm connection bolts and those without a diaphragm connection indicated nearly the same fatigue life.
- Web-gap strains and out-of-plane displacement showed variation with truck speed and the location of the truck in the transverse position.
- For the k-type diaphragm system, the maximum distortion occurred at an interior girder (not an exterior one), as diaphragms are discontinuous leaving exterior and interior girders with equal opportunities of distortion
- Out-of -plane displacements associated with using a k-type diaphragm system were substantially less than those in x-type diaphragm system. This was due to:
    - The smaller length of the web-gaps that affected the magnitude of the out-of-plane displacement.

- The reduction in the horizontal force transmitted through the upper chord of the k-type diaphragm located near the top flange of the girder.

Wipf, et al. [9] used continuous remote monitoring system to investigate the bolt-loosening retrofit over a time period to ensure that the measured strain and displacement reductions are not affected by time and repeated traffic loading.

In 2001, Roddis and Zhao [5] studied the causes and suggested several repair methods to minimize the distortion in the web-gap region in steel bridges. The following were some of the repair alternatives recommended in Ref. [5].

- Filling drilled holes with pretension bolts could be used to prevent crack initiation from the drilled holes in cases of high stress intensity factors around these holes.
- Stiffening the web-gap by connecting the stiffener plate to the flange of the girder using welded or bolted connections.
- Welding the web stiffener to the girder flange was found to resist stress ranges up to AASHTO fatigue detail category C whereas a bolted connection plate detail was found to improve fatigue resistance to AASHTO fatigue detail category B.

- Using bolted spliced plate in cracked web-gap regions were found to improve the load carrying capacity of the main structural member if large fatigue cracks have been developed and propagated into the girder web.
- Cutting part of the connection plate so that the area of the girder below the flange is sufficiently flexible to accommodate the out-of-plane rotation improved web cracking formation due to out-of-plane distortion. However, the cut section should be well finished to prevent crack initiation.
- Using composite materials such as pre-stressed carbon fiber laminates oriented perpendicular to the crack orientation could slow down or even completely stop crack propagation.

In 2003, Roddis and Zhao [7] used finite element modeling techniques to identify the location of potential crack initiation and to determine the corresponding distortion-induced stresses in the web-gap region of continuous steel girder bridges. Coarse finite element model considering only the central span was utilized in the analysis assuming fixed supports at both ends of all girders. An HS 15 fatigue truck was placed at 20 different locations. Sub-models of the region at mid-span of the girder including bottom and top flange then utilized by Roddis and Zhao [7] were analyzed to get more accurate results. The authors of Ref. [7] recommended

using bolted or welded stiffener-flange connections as a repair method in the positive and negative moment regions. In addition, an out-of-plane stress-displacement correlation was formulated from the findings of the analytical results which was suggested by Roddis and Zhao [7] to serve as a simple approach for web gap stress prediction.

In a related study by Roddis and Zhao [6], a finite element analysis modeling was developed to describe the behavior of web-gap crack development, and to assess the effectiveness of different repair alternatives. A two-girder, non-skewed bridge with a truss system for the floor beams was studied. Three finite element models representing positive and negative moment regions of a girder were considered. Length of each model is equal to the spacing between the floor beams. Several retrofit alternatives range from removal of diaphragm, and/or adding new stiffener plate or a combination of these were investigated. The study concluded that the repair method used in the positive moment region was unsatisfactory for the negative moment region, and hence additional floor truss member removal was recommended.

In 2003, Jajich and Shultz [3] conducted a study on the frequency and magnitude of distortional fatigue stresses at web-stiffener connections in steel bridges. The impact of stresses on fatigue life of the bridge girders

was also investigated. Experimental and finite element analyses were carried out. The finite element model considered only two of the adjacent girders connected by a diaphragm and extending to the nearest diaphragm or pier. The bridge deck was not included in the model and the girder top flanges were assumed to be rotationally fixed due to the presence of the deck. The model was loaded by prescribing vertical displacements that were obtained from the experimental test. The finite element model results were compared with measured values and a simple technique for predicting the stresses in the web-gap were developed. Fatigue life calculations using the experimental data were also made.

The work presented herein is part of a project sponsored by the Iowa Department of Transportation (DOT) the objective of which was to investigate the effects of welding the stiffener plate to the top flange of a steel girder on reducing the stresses in the web-gap region.

2. FIELD TESTS OF A SKEWED BRIDGE

2.1 Introduction

Field tests were conducted on a multi-girder steel bridge to investigate the strain concentration in the web-gap region. The results of the field test were utilized for the development of the finite element model and its calibration. Since investigation of the web-gap distortion phenomenon of the bridge using finite element methods was the main objective of this research, it was necessary to confirm the accuracy of the finite element results using the field tests. This chapter describes in detail the various components of the bridge that was studied, the test set-up and the load configurations utilized in the test.

2.2 Bridge description

The bridge studied for distortion-induced damage is located in Black Hawk County, Iowa. The bridge, designated as Design No.1283, is built on county road D-180 that crosses over I-380. The bridge has four spans and a skew angle of $46^0 41'24''$. Going in the east direction, the first span is 69ft. long; the second and third spans, each is 128ft. long, and the fourth span is 72 ft. long. The super-structure on this bridge consists of an eight in. thick reinforced concrete slab supported by five steel plate girders. The super-structure is supported on three piers and two abutments. Several views of the bridge are shown in Figs. 2.1to 2.5.

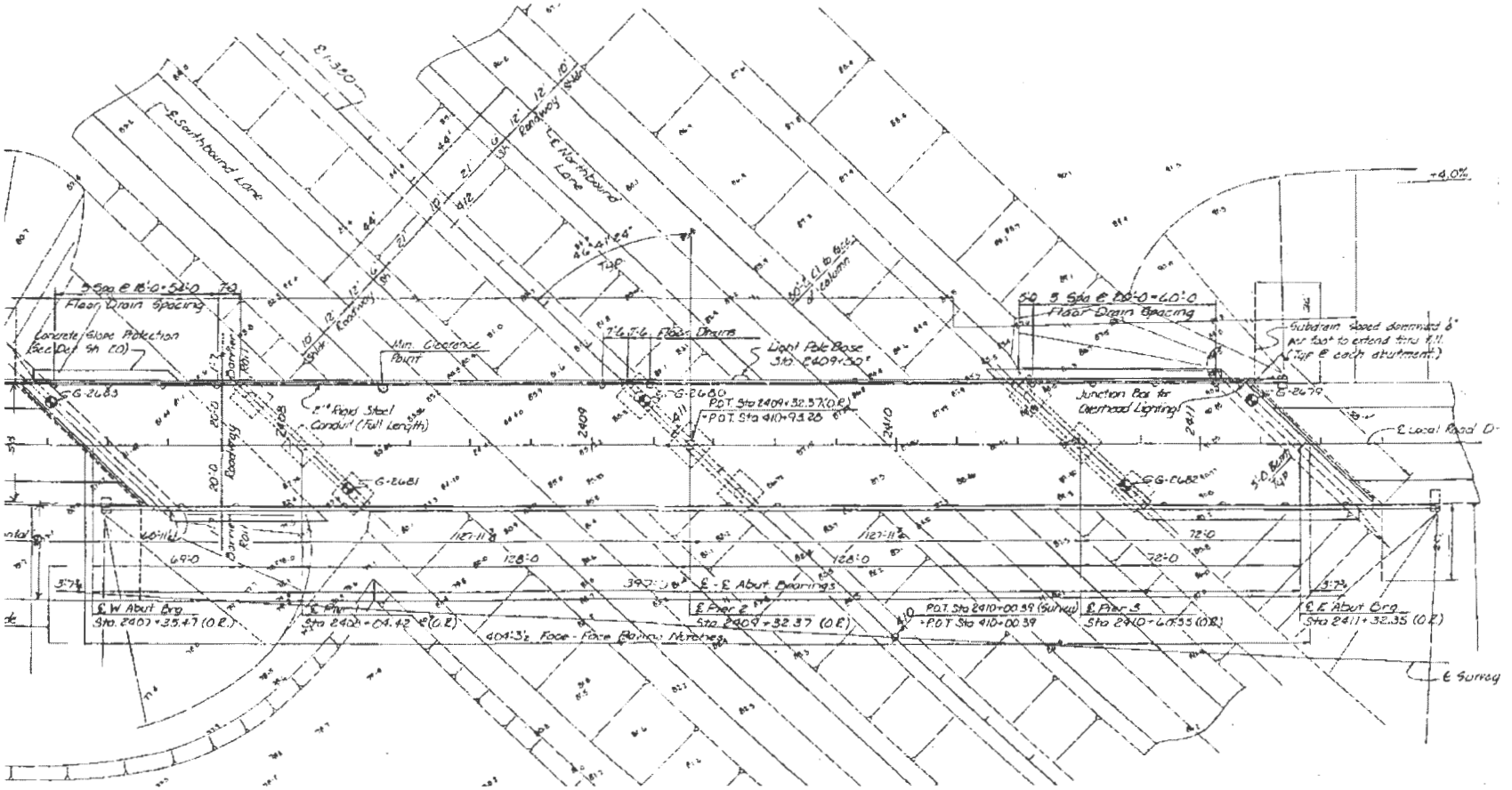

Figure 2.1 Situation plan (Adapted from Iowa DOT-Highway Division design details, File no. 25779, Sheet no. 21)

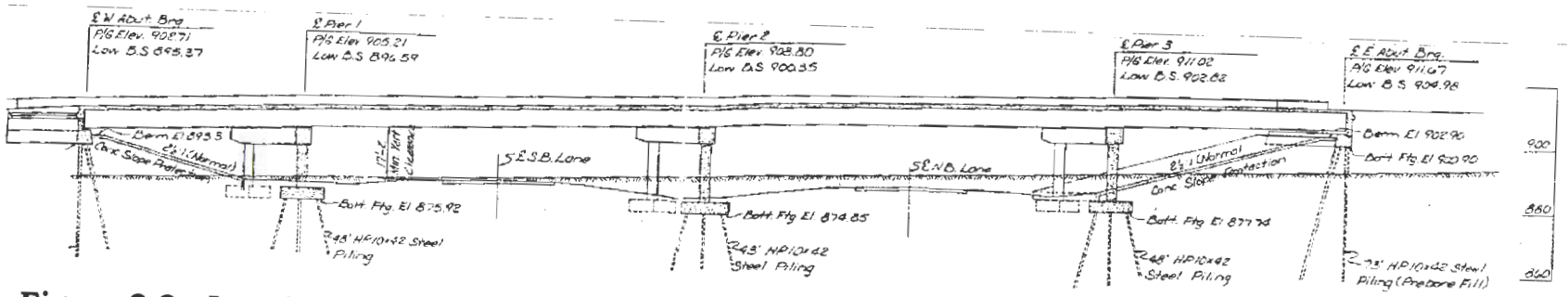

Figure 2.2 Longitudinal section along centerline of road (Adapted from Iowa DOT- Highway Division design details, File no. 25779, Sheet no. 21)

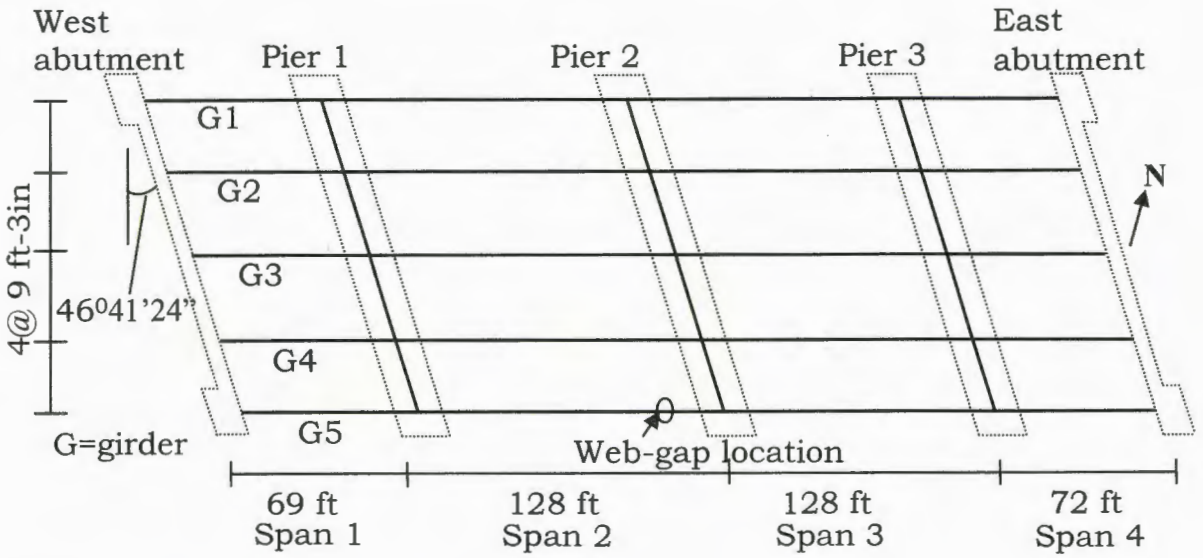

Figure 2.3 Plan view of bridge super-structure

Figure 2.4 Overview of the bridge

Figure 2.5 General view of the roadway

2.2.1 Bridge girders

As previously mentioned the bridge deck is supported on five steel plate girders. A typical girder is composed of different plates with the cross-sectional dimensions as shown in Figure 2.6. The web of all girders is built using 60" x 3/8" plate throughout the girder length. However, the dimensions of the top flanges vary along the girder length as listed in Table 2.1. The dimensions of the bottom flange are similar to the top flange except that the 17" x 1" section is replaced by a 12" x ¾" section.

Table 2.1 Top flange dimensions across the girder

Dimensions (in.)	Range from left abutment (ft.)
10x 3/4	0-35 & 368-407
$17x1\frac{1}{2}$	35-104 & 310-368
12x3/4	104-170.75& 243.25-310
20x1	170.75-192 & 222-243.25
$20x1\frac{15}{16}$	192-222

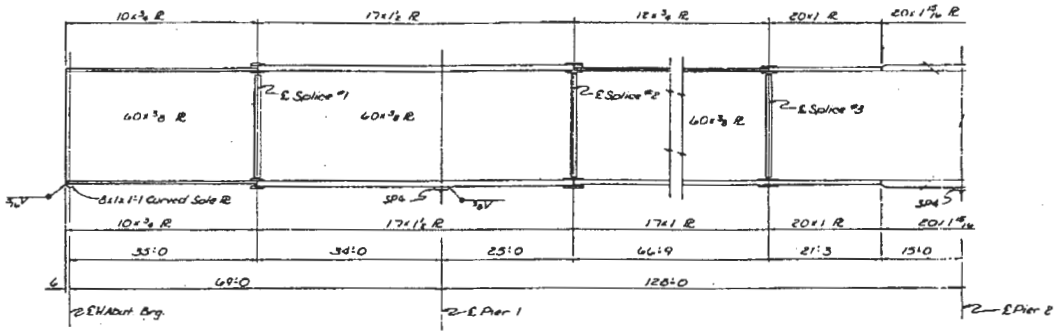

a. Girder details between the west abutment and a distance of 222 ft

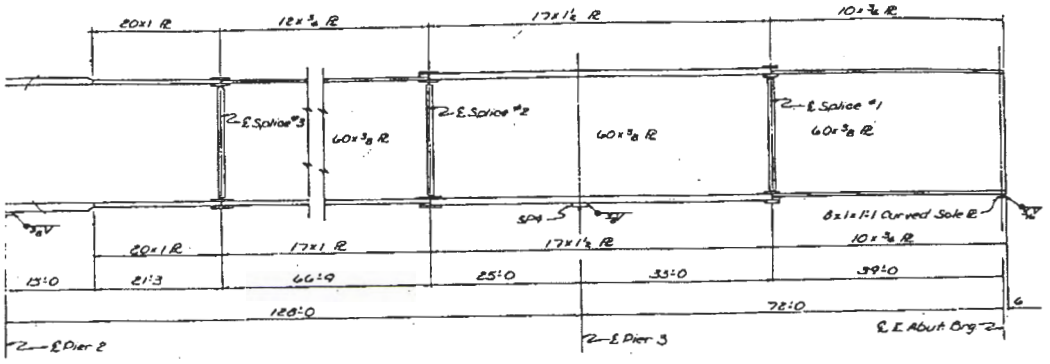

b. Girder details between distances of 222 ft and east abutment

Figure 2.6 Typical girder details (Adapted from Iowa DOT-Highway Division design details, File no. 25779, Sheet no.32)

2.2.2 Diaphragms and web stiffeners

The five girders in the bridge structure are connected by x-type diaphragms as shown in Figures 2.7 to 2.9. The cross-sections near abutment, positive and negative moment regions are shown in Figures 2.7 and 2.8. As can be noticed, W 24x68 floor beams are used near the abutments (Fig. 2.7). The x-type diaphragms are composed of L 4"x3"x5/16" and WT 4x9 steel sections as shown in Fig. 2.7. These are attached to the web-stiffeners using bolted connections. A photo showing a view from beneath the bridge deck is shown in Fig. 2.9.

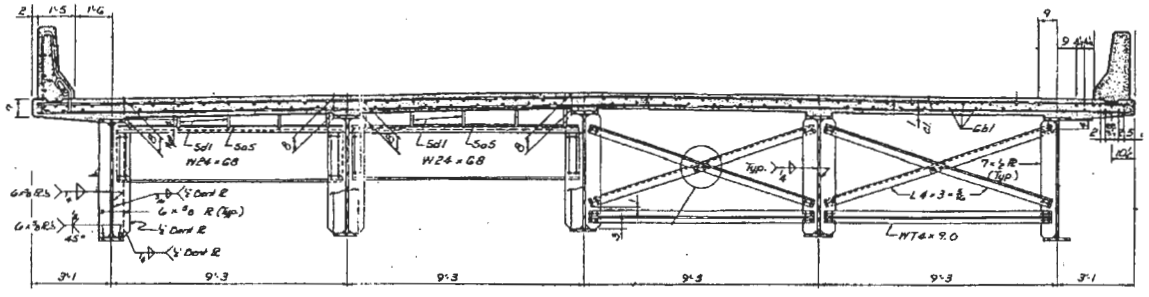

Figure 2.7 Half sections near abutment and in positive moment regions (Adapted from Iowa DOT-Highway Division design details, File no. 25779, Sheet no.30)

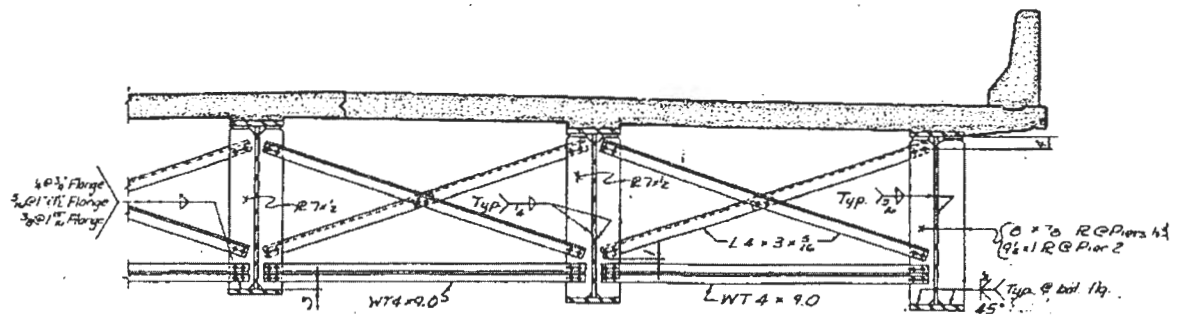

Figure 2.8 Half section in negative moment region (Adapted from Iowa DOT-Highway Division design details, File no. 25779, Sheet no.30)

Figure 2.9 Photo from underneath the bridge showing diaphragm system

Examining the bridge structure shows that, in the negative moment region, the web-stiffeners are connected to the top flange of the girder by ½" thick plates. Fig. 2.10 shows a bolted plate connecting the web-stiffener to the top of the flange of the girder. The details of the connection between the web stiffener and the top flange in the negative and the positive moment regions are shown in Figures 2.11 and 2.12, respectively.

Figure 2.10 Bolted plate connecting stiffener to top flange of girder

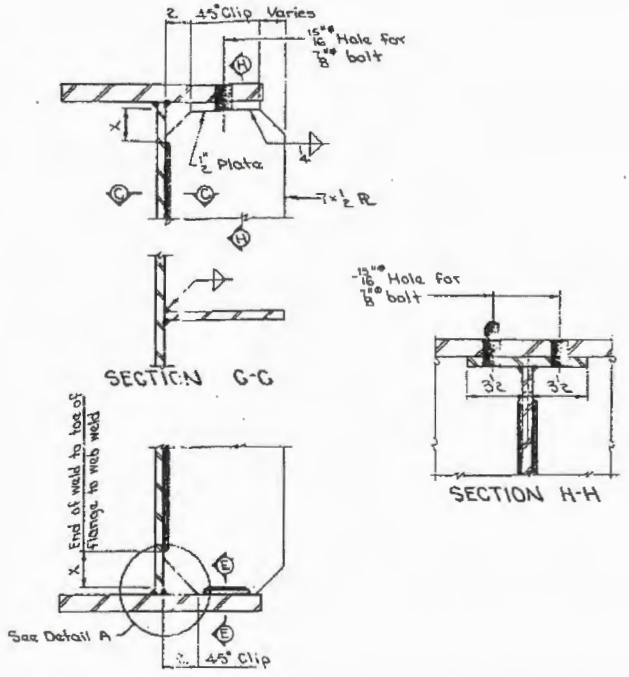

Figure 2.11 Details of stiffener-web connection in the negative moment region (Adapted from Iowa DOT-Highway Division design details, File no. 25779, Sheet no.36)

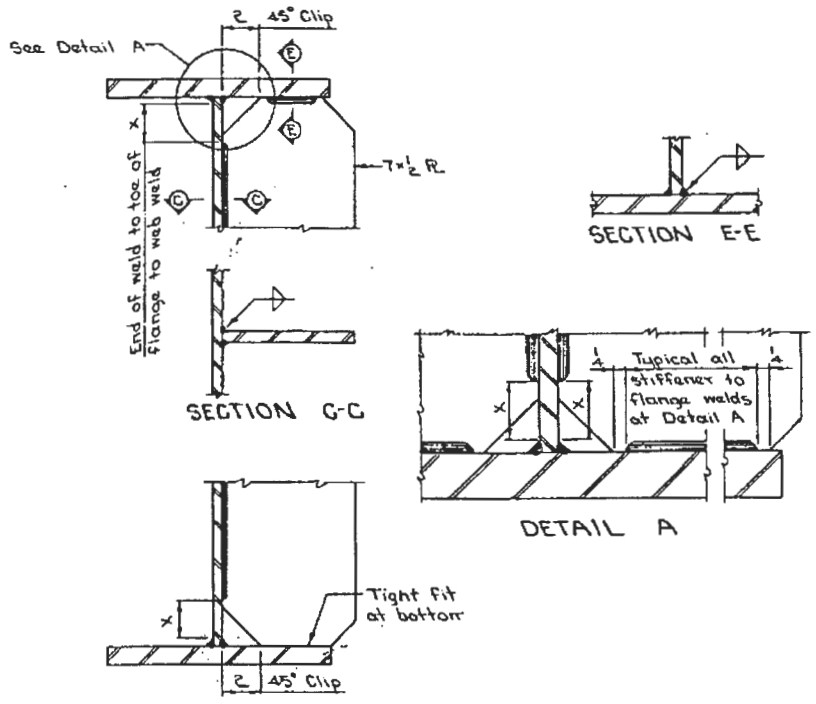

Figure 2.12 Details of the stiffener-web connection in the positive moment region (Adapted from Iowa DOT-Highway Division design details, File no. 25779, Sheet no.36)

2.2.3 Web-gap details

The web-gap investigated herein is located near the middle pier as shown in Fig. 2.3. Figures 2.13 and 2.14 show that the length of the gap measured from the top of the fillet weld of the flange of the girder to the top of the fillet weld of the web-stiffener connection is 2.75 inches. The top size of the weld connecting the web to the top flange is 0.3125 in. thick.

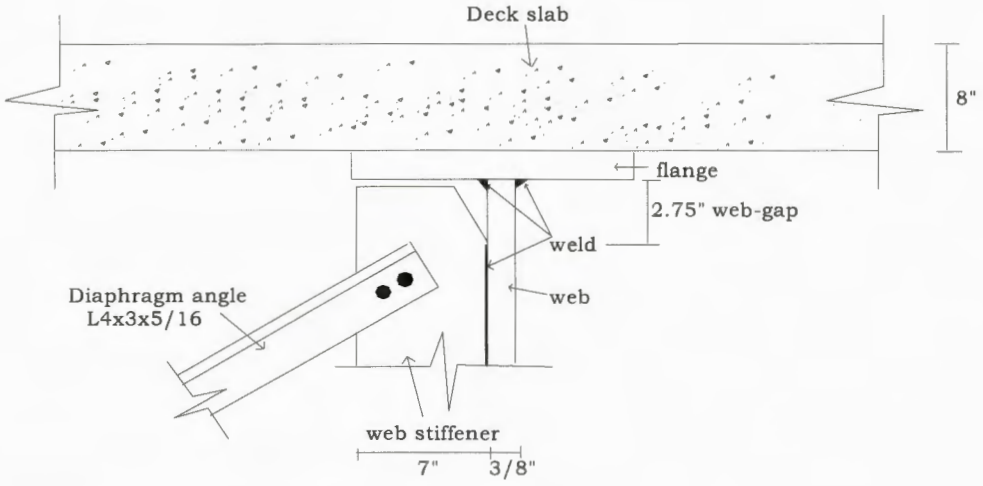

Figure 2.13 Details of the web-gap region

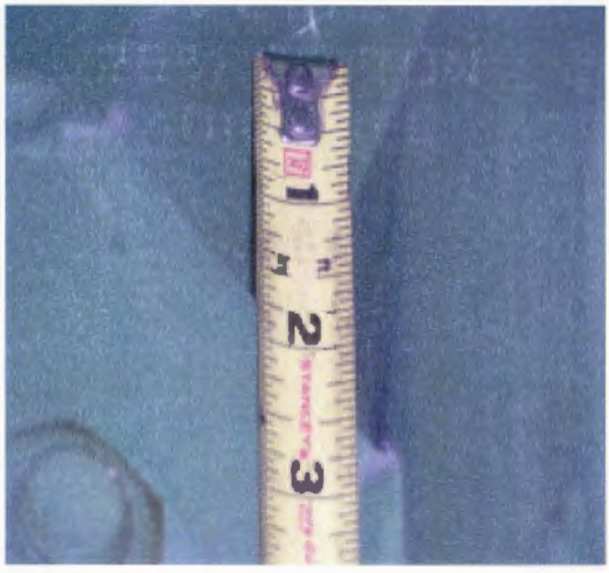

Figure 2.14 Photograph of web-gap

2.3 Instrumentation

The field test involved mounting of strain-gages at two locations of interest. The first set of strain-gages was placed within the web-gap region. The other strain-gages were placed on the legs of the x-diaphragm that is connected to the web-stiffener at the web-gap region.

2.3.1 Web-gap instrumentation

Five strain-gages were placed over an 11/16" height, the top being positioned approximately at 13/16 in. from the bottom of the top girder flange. These strain-gages were placed at 3/4" offset to the right side of the stiffener face (Fig. 2.15).

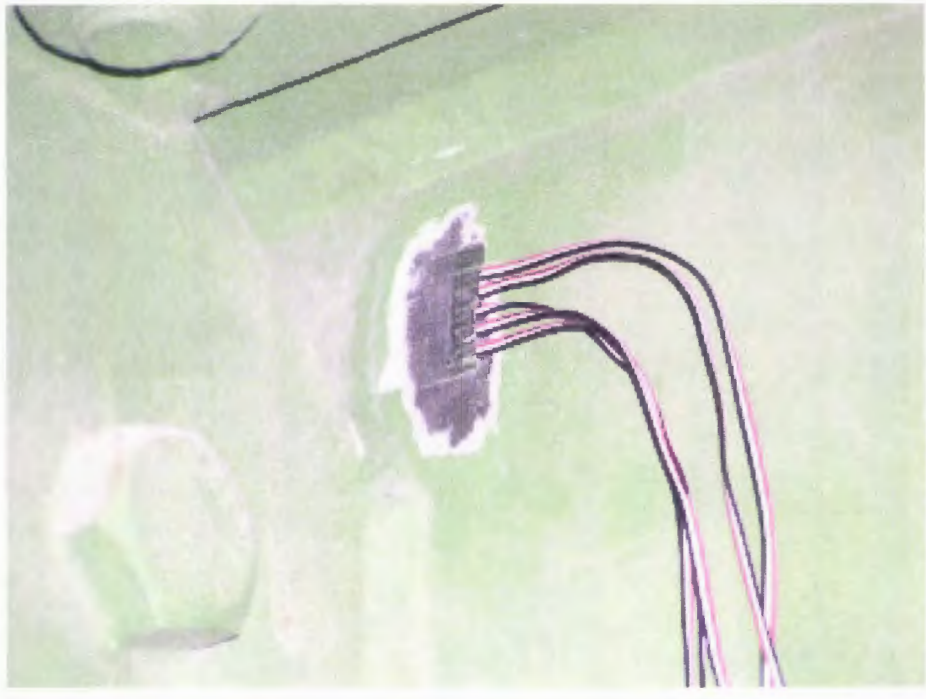

Figure 2.15 Strain-gage arrangements in web-gap

2.3.2 Diaphragm instrumentation

The layout of the instrumentation on one member of the diaphragm assembly is shown in Figures 2.16 and 2.17. As shown in Figure 2.16, three strain-gages were placed at a distance of 27 in. from the bolts connecting the x-bracing to the stiffener. These gages were used to measure the strains induced in this member when a differential deflection between the two girders takes place as a load travels over the bridge.

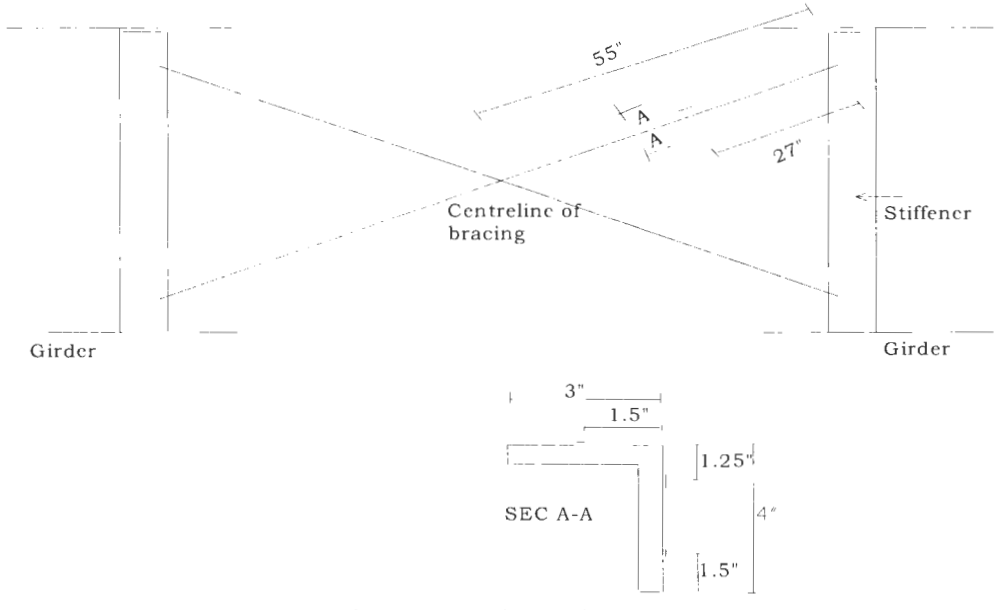

Figure 2.16 Layout of instrumentation on the cross-bracing

Figure 2.17 Diaphragm instrumentation

2.4 Loading

2.4.1 Loading description

Two trucks were used in loading the bridge for the field test. Figure 2.18 shows a similar configuration as one of the eight loading arrangements that was used in testing the bridge structure. The magnitudes of the front and rear axle wheel loads as well as the dimensions of the two trucks used in the bridge test are shown in Figure 2.19.

2.4.2 Loading cases

There were total of eight loading cases that were considered during the field test of the bridge. The first four cases had the trucks driving to the west, while the last four cases heading to the east. The arrangements of

these eight load cases are shown in Figures 2.20 and 2.21. Two locations that correspond to known load positions for strain readings are marked as m1 and m2 as shown in Fig. 2.21.

Figure 2.18 Truck arrangement used for tests on similar bridges

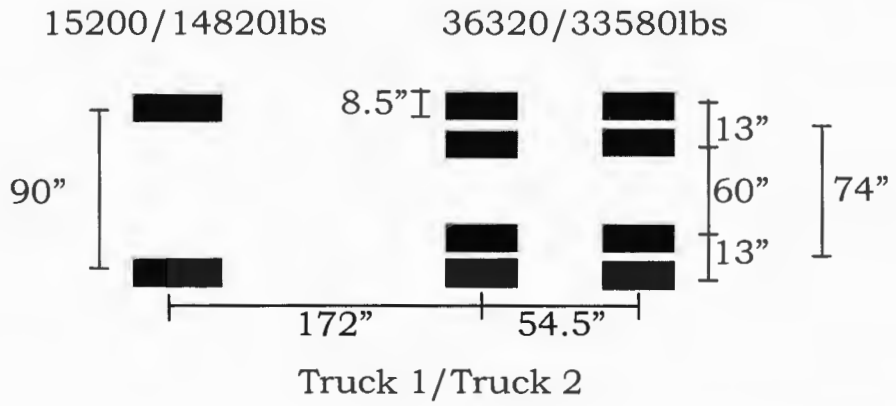

Figure 2.19 Test trucks axle load distribution

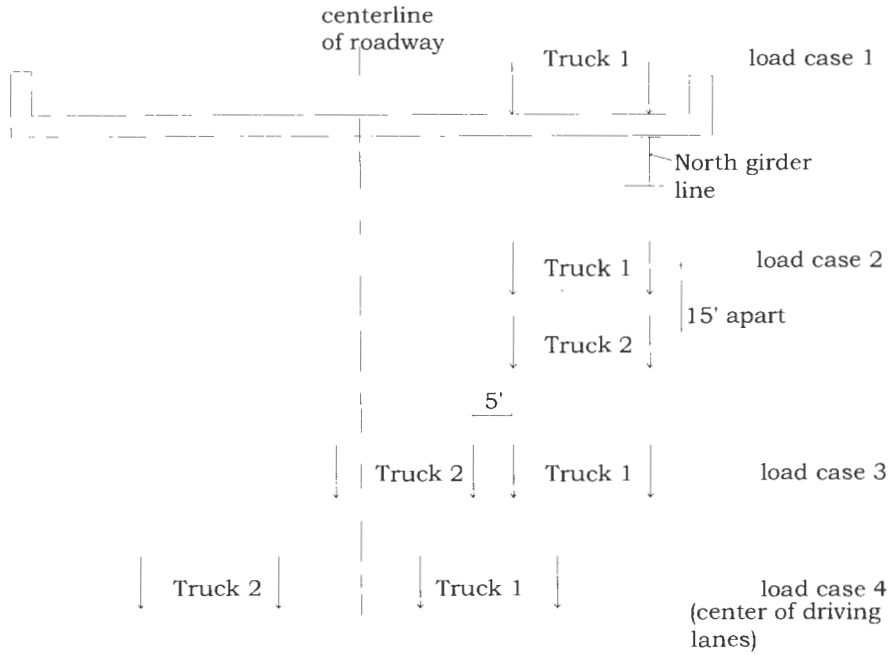

a. Load cases 1-4: looking west, trucks driving west

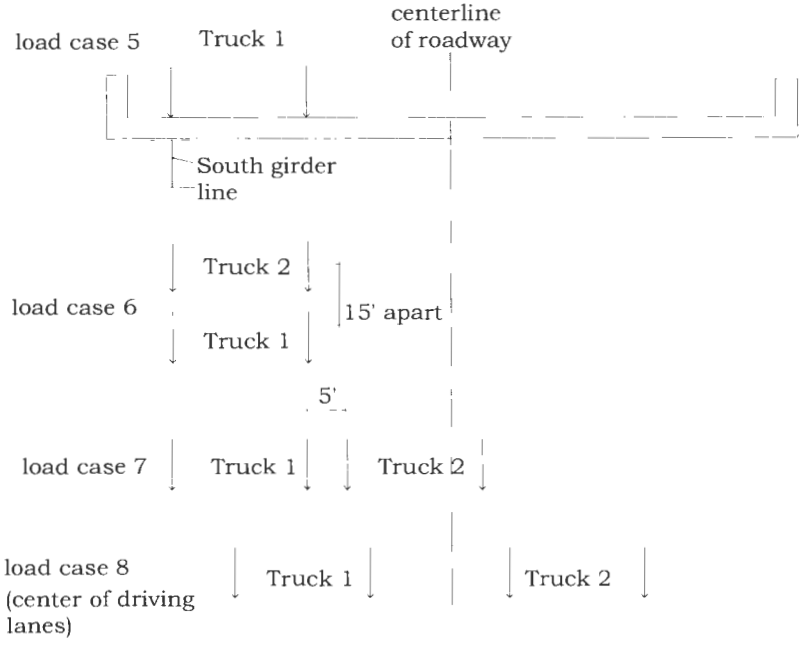

b. Load cases 5-8: looking west, trucks driving east

Figure 2.20 Transverse load case configurations

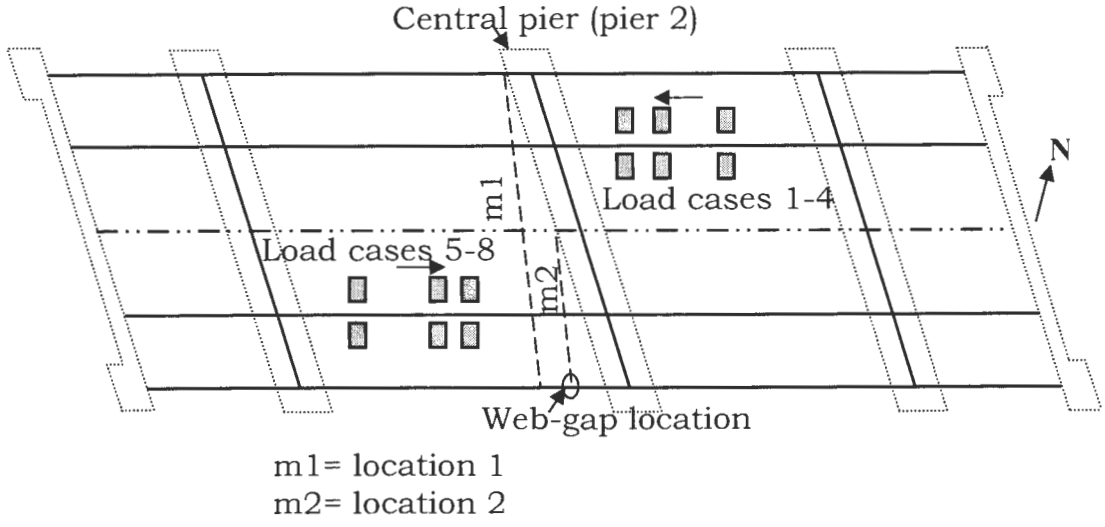

Figure 2.21 Plan view of load case configurations

3. FINITE ELEMENT MODELING OF A SKEWED STEEL BRIDGE

3.1 Introduction

As previously mentioned, crack formation in the web-gap region in steel bridges is a complex phenomenon. Review of published literature indicated that there had been no closed form solutions for determining the stresses and strains that are caused by local distortion in the web-gap region in steel bridges. Instead, finite element analysis had been adopted to calculate the stresses and strains in such a region. In the work presented herein the distortion in the web-gap, and different retrofit alternatives that can be used to reduce or eliminate the distortion and hence reduce stress concentration have been investigated using the finite element technique. This was accomplished by analyzing several three dimensional models of the steel bridge that was described in the previous chapter using the ANSYS software [2]. Several finite element packages are available at Iowa State University, for instance, ANSYS, ABAQUS and STAAD. The ANSYS software was selected in this study, primarily because of its convenient pre- and post-processing features.

ANSYS is a large-scale, user–oriented, general purpose finite element program for analyzing linear and non-linear structures under static, dynamic, creep and thermal loading. The program contains a library of several elements that could be used to model structures with complex

geometry. In addition, ANSYS provides a Graphical User Interface (GUI) for the pre-and post-processor phases. This option enables the user to continuously check the input during the course of developing a finite element model and to represent analysis results in different formats. For example, plots of the deformed shape, stress or strain contours of the finite element analysis can be easily retrieved using the different post-processing options available in the ANSYS program.

3.2 Description of the finite element model

For the bridge under study the solid-modeling option available in the ANSYS software was used. Solid-modeling is one of the two methods for generation of elements, the other being direct generation of nodes and elements. The solid-modeling was selected due to the complexity in geometry and details of the structural members of the bridge. Modeling such a complex structure using node and element generation would have been quite cumbersome.

In the ANSYS program, solid models can be created in two ways:

1. Top-down construction: this implies that volumes and areas that represent the different components of a bridge system are created directly.

2. Bottom-up construction: in this case sequential creations of basic components of a structure are built using the solid-modeling. This is accomplished by defining key points, lines, areas, and volumes. In this work, the bottom-up construction solid-modeling approach was used, and the steps followed to create a finite element model of the skewed bridge discussed in chapter 2 are explained in details in the following sections.

Perhaps the single most important step in solid-modeling a structure is to plan beforehand what line divisions will be used at different locations for different components of the finite element model. This is essential so that when meshing is done, nodes on common lines among different components, which are supposed to be connected together, actually end up at the same location. Otherwise, it may later result in the creation of unaligned nodal points during element formation by meshing.

As was previously stated, the bridge investigated herein consists of four spans with web-gaps located in the two interior spans. Traffic loads acting on the two outer spans, i. e., remote from the web-gap, have inconsequential effects on the out-of-plane distortion of the web-gap near the middle pier. In addition, the availability of computer storage space and the need the reduction in the analysis time without sacrificing the accuracy

of the results, are also factors that one needs to consider when carrying out an analysis of a large size model. Therefore, one may select to model the middle two spans only for the finite element analysis. Furthermore, to ensure accurate modeling for the behavior on the local distortion at the web-gap region, one needs to use fine mesh. This can be achieved using the H-refinement option available in the ANSYS program. However, utilizing this approach would result in unreasonable solution time. Another alternative is to use the sub-modeling option provided in the program. In this case, one needs to first model the two spans of the bridge structure using a reasonably coarse mesh. In the next step, a model that includes the web-gap and small portion of the bridge structure in its vicinity is constructed and analyzed with its boundaries subjected to the results obtained from the coarse model. This approach was pursued in this work to investigate the stresses and strains in the web-gap region.

3.2.1 Coarse model

As shown in Fig. 2.3, the two interior spans of the bridge structure are geometrically symmetrical. Therefore, it was sufficient to model only one span of the bridge and then utilize the copy command provided in the ANSYS software to construct the finite element model of the other span.

The span of the bridge that was considered for the initial solid-modeling was divided into five components for building the solid models. These components comprised of the bridge deck, girders, diaphragms, web-stiffeners and connection plates. The development of the solid models and the attainment of the elements for these components are presented below.

3.2.1.1 Modeling of the bridge girders

The solid-modeling of the bridge girder started with defining lines with key-points to form the cross-section of the girder. Areas were then created by extruding lines along the longitudinal direction of the girders. This facilitated the creation of the girders since there were many areas that needed to be separately formed due to changes in cross-sectional dimensions of the bridge girders (See Fig.2.6).

Once the over all shape of a girder was created, commands were then issued to create the mesh using a user specified element size. Plate elements that are referred to as shell 63 in the ANSYS element library were used. The weld connecting the girder flanges to the web was modeled with shell elements that have variable thicknesses. Figure 3.1 shows a portion of the meshed girder. The created mesh for this girder was replicated at the locations of the other girders using the copy command available in the ANSYS program.

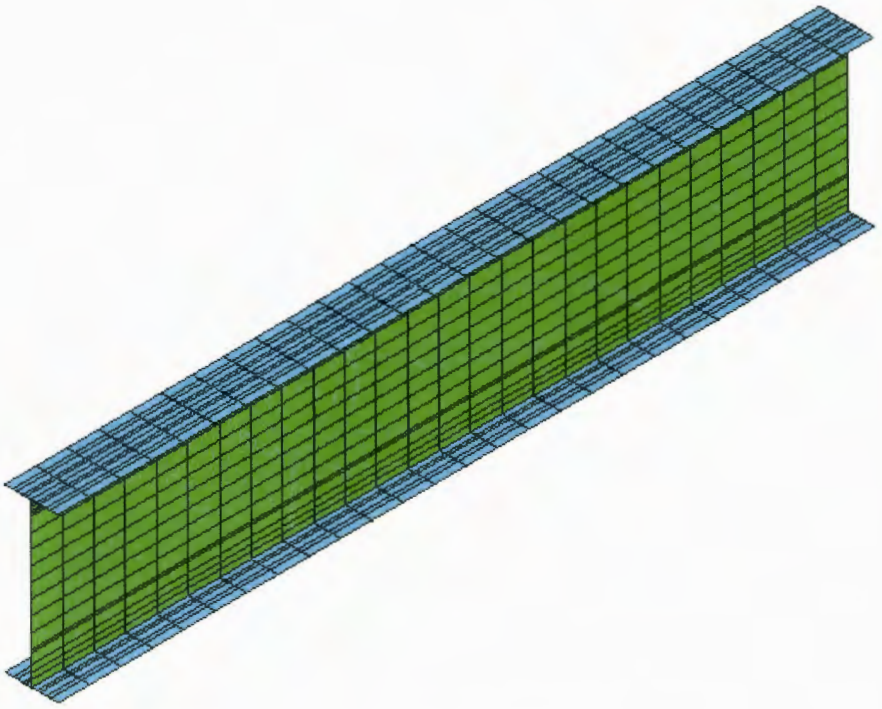

Figure 3.1 Isometric view of a portion of the girder

3.2.1.2 Modeling of the diaphragms

As shown in Figs. 2.7 and 2.8, two different stiffener-diaphragm systems were used in the positive and negative moment regions. In addition, these figures show that additional plates were added to connect the stiffener in the negative moment regions to the top flange of the bridge girder, while the other end of these stiffeners were directly connected to the bottom flange. In the positive moment regions, the top end of the stiffeners was connected with the top flange, whereas the bottom of the stiffener was fit in tight to the bottom flange of the girder.

Solid-modeling was used to model the diaphragm system of the bridge structure. First a finite element model for the stiffener system in the negative moment region was constructed. The different components of the diaphragm system, i. e., the vertical stiffener and the cross bracings were created and meshed using shell elements. Common nodes were used to ensure correct connections between these components. Once the stiffener-diaphragm model was built, it was stored for later retrieval to be included in the overall finite element model of the bridge. This model was also modified to include the geometrical details of web-stiffener of the diaphragm in the positive moment region. The model for the stiffener in the positive moment region was also stored for future use to construct the over all model of the bridge structure. Figures 3.2 and 3.3 illustrate the finite element model of the diaphragm systems in the negative and positive moment regions, respectively. A portion of the finite element model showing the bridge girders, the web-stiffeners and the diaphragms is illustrated in Fig. 3.4.

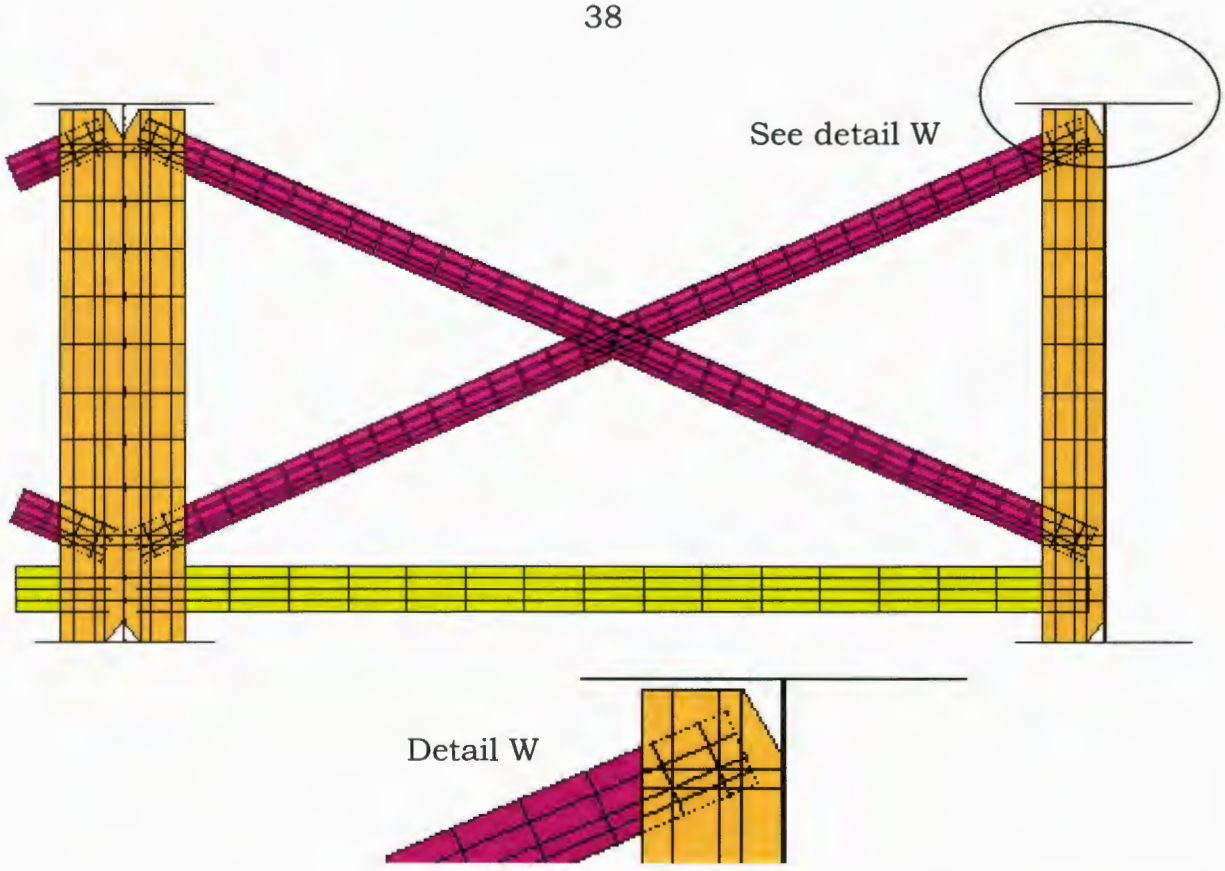

Figure 3.2 Negative moment region stiffener-diaphragm

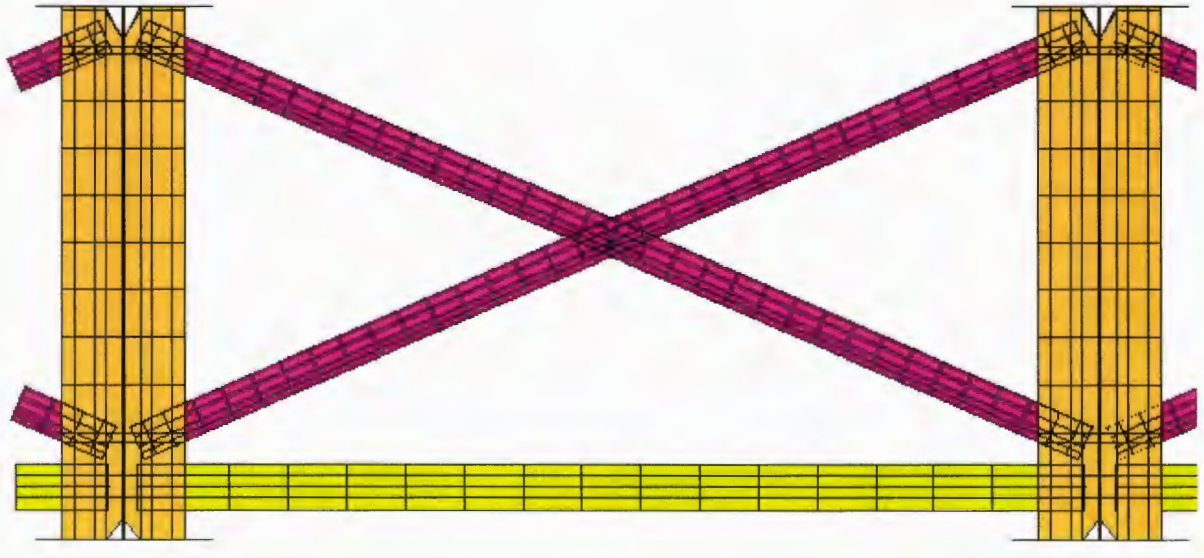

Figure 3.3 Positive moment region stiffener-diaphragm

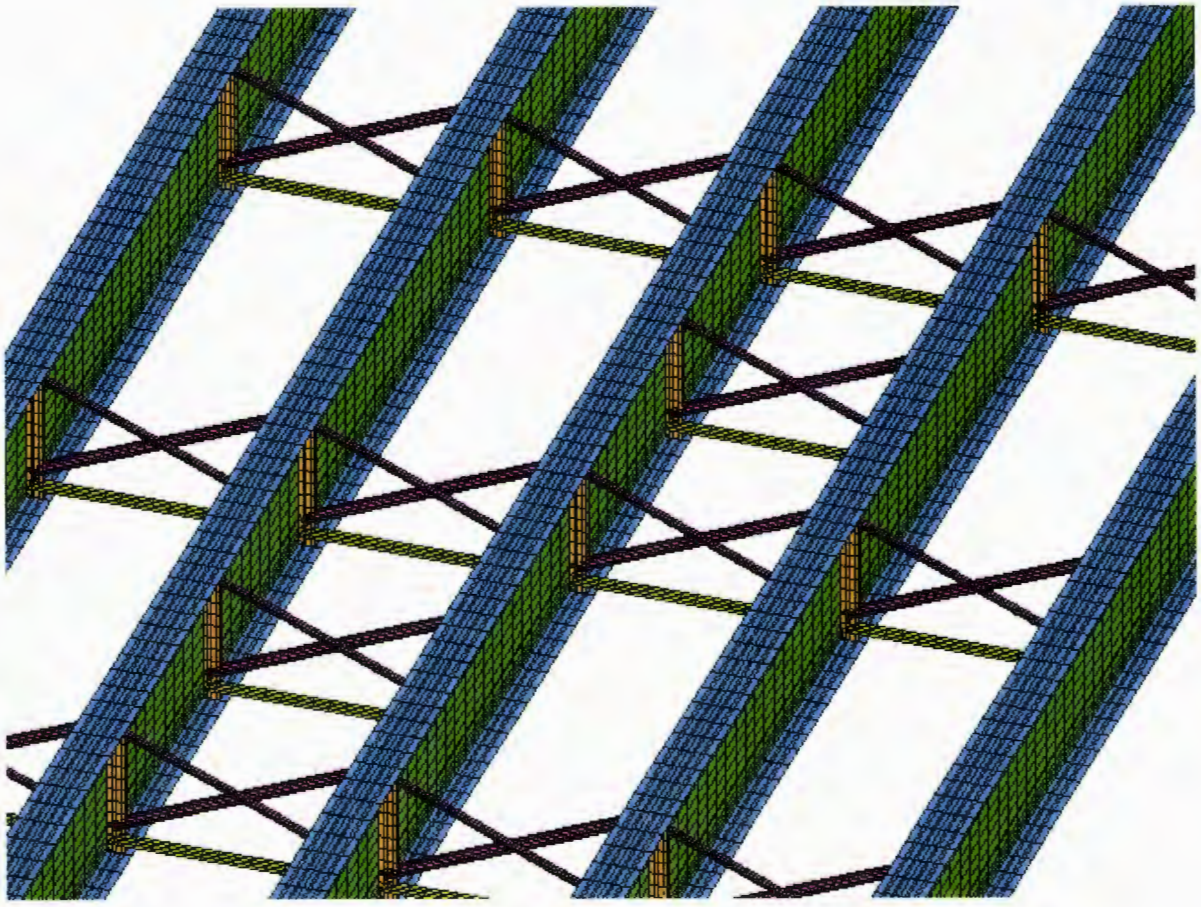

Figure 3.4 Isometric view of portion of girder-stiffener-diaphragm elements

3.2.1.3 Modeling of the bridge deck

The bridge deck was also modeled using the solid-modeling technique. The deck centerline portions directly above the girders were created by copying the girder top flange areas at a distance equal to half of the thickness of the deck. Once these deck portions were created, key points at their corners were used to define the boundaries for the rest of the deck, i.e., the portions between the girders. Additional areas that represent the triangular portions resulted from the skewness of the bridge and were

created separately. All areas were merged together and were then meshed using plate elements. Finally the copy command available in the ANSYS program was issued to create the finite element mesh of the second span. The finite element mesh of a portion of the bridge, which also includes the bridge deck mesh, is shown in Fig.3.5.

3.2.1.4 Girder-deck connection

As described above, plate elements were used to model the deck and the girders of the bridge structure. In this case, a gap between these two bridge components would exist since these plate elements were defined by nodes that were located at the center of these components. To connect the bridge deck to the bridge girders, rigid link elements were used. This was defined in ANSYS using constraint equations with the nodes along the flange and the deck labeled as master nodes and slave nodes, respectively (see Fig. 3.6)

3.2.1.5 Support conditions

The ends of the two spans representing the cut sections near piers opposite to the central pier were modeled by imposing fixed boundary conditions at these locations. The support provided by the central pier was modeled as a roller support that restrained the displacement in the direction perpendicular to the plane of the deck (See Figure 3.7).

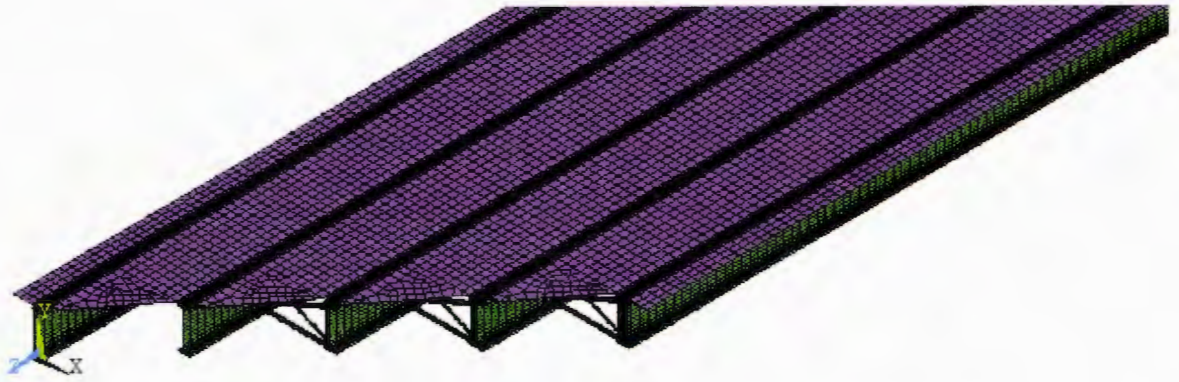

Figure 3.5 Finite element mesh for a portion of the bridge

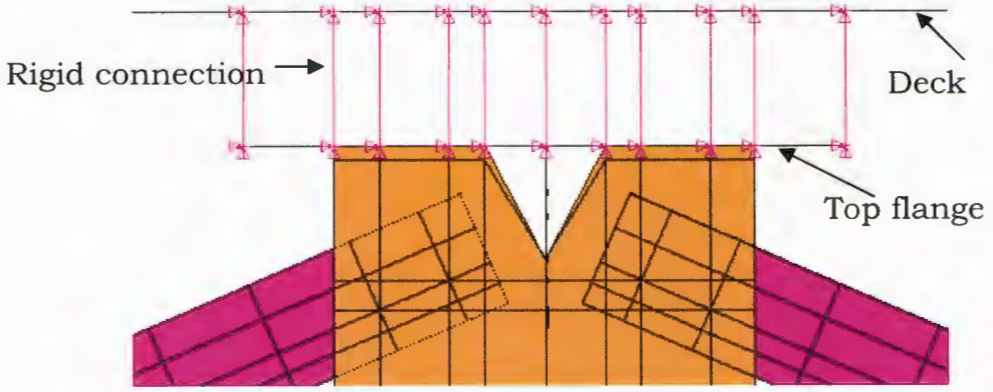

Figure 3.6 Top flange-deck rigid connection

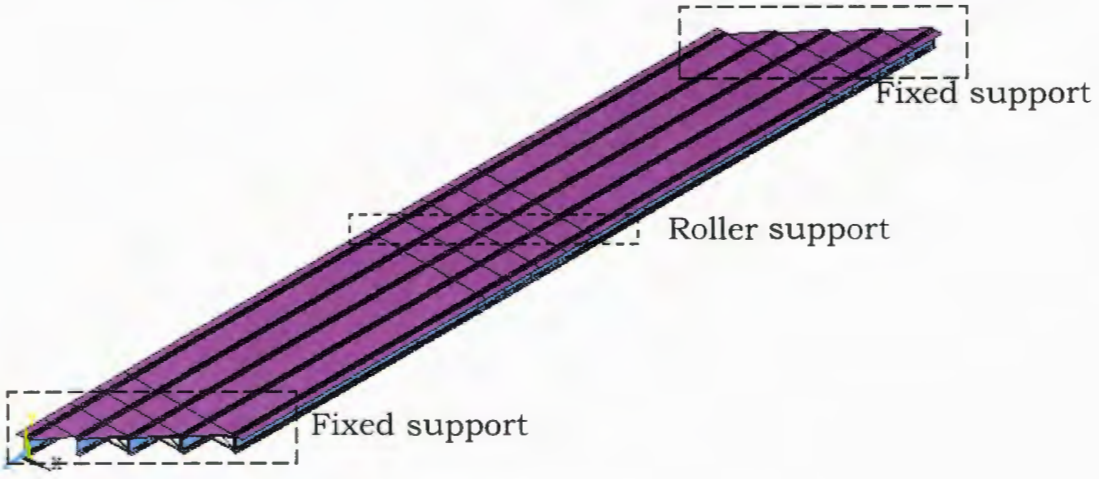

Figure 3.7 Support conditions for the bridge

3.2.2 Sub-modeling

3.2.2.1 Sub-model description

The web-gap under investigation is located near the central pier. The coarse model in the vicinity of this region had, on average, plate elements with a length of 12 in. used in the longitudinal direction of the bridge. This was believed to be too coarse to produce satisfactory results and to accurately model the behavior of the web-gap region. Moreover, using elements with this size in the web-gap region did not coincide with the spacing of the strain gages that was utilized in the field test and would not allow direct comparison between the analytical and field test strain results. Therefore, to obtain more accurate results, it was necessary either to re-analyze the entire model with greater mesh refinement or generate an independent, finer meshed model of the web-gap region only, i.e., using the sub-modeling option in the ANSYS program. As can be seen, the first option was not found to be practical as it would be time-consuming and uneconomical. Therefore, it was decided to use the sub-modeling technique to further investigate the strains and stresses in the web-gap region.

Sub-modeling, also known as the cut-boundary displacement method, is a technique that develops a sub-model having a boundary representing a cut through a coarse model. The boundary conditions to be applied to the sub-model are the displacements computed at the cut boundary obtained

from analyzing the coarse model of the entire structure considered for modeling.

The principle behind sub-modeling is the St. Venant's principle, which states that if an actual distribution of forces is replaced by a statically equivalent system, the distribution of stress and strain is not altered at locations remote from regions of load application.

In this study, the sub-model of the web-gap region included portions of the bridge deck, bridge girder, stiffener plate and cross bracing. A sensitivity study was conducted to determine the size of the sub-model that can be used in the analysis. This was accomplished by comparing the results obtained from the sub-model near the cut boundaries with those obtained from the coarse model. In addition, the effect of the location of the cut-off boundaries on the stress and strain results was also investigated. The sensitivity study showed that including a portion that is 25 in. long on each side of the stiffener would be enough to accurately analyze the web-gap region (See Fig. 3.8).

The size of the elements used to idealize the components included in the sub-model was limited to 0.25in by 0.25in. The total number of elements in the sub-model was about 50,000. Worthy to mention that using elements with smaller size to model the girder plate in the web-gap

area was also investigated; however, the difference in the results was negligible. Hence, it was decided to maintain an element size of 0.25in x 0.25in.

The sub-model built was modified to represent the different alternatives that were part of this study. The as-built structure has a plate connecting the stiffener to the top flange. One of the other retrofits considered was the addition of external stiffener and hence the sub-model was modified to represent condition. Figures 3.8-3.10 show some views of the sub-models described above.

3.2.2.2 Modeling the connections between various components

Nodes corresponding to the top flange of the girder and the deck were connected using rigid links as those in the coarse-model. However, unlike the coarse model, the region between the centerline of the flange and the top of the weld was modeled using rigid links with the nodes along the girder flange were specified as master nodes.

The connection plate that connects the web-stiffener with the top flange of the girder was modeled by shell elements. Rigid links were used to connect this plate with the flange of the girder. In this case, the connection plate nodes were the ones with master degrees of freedom, while the nodes

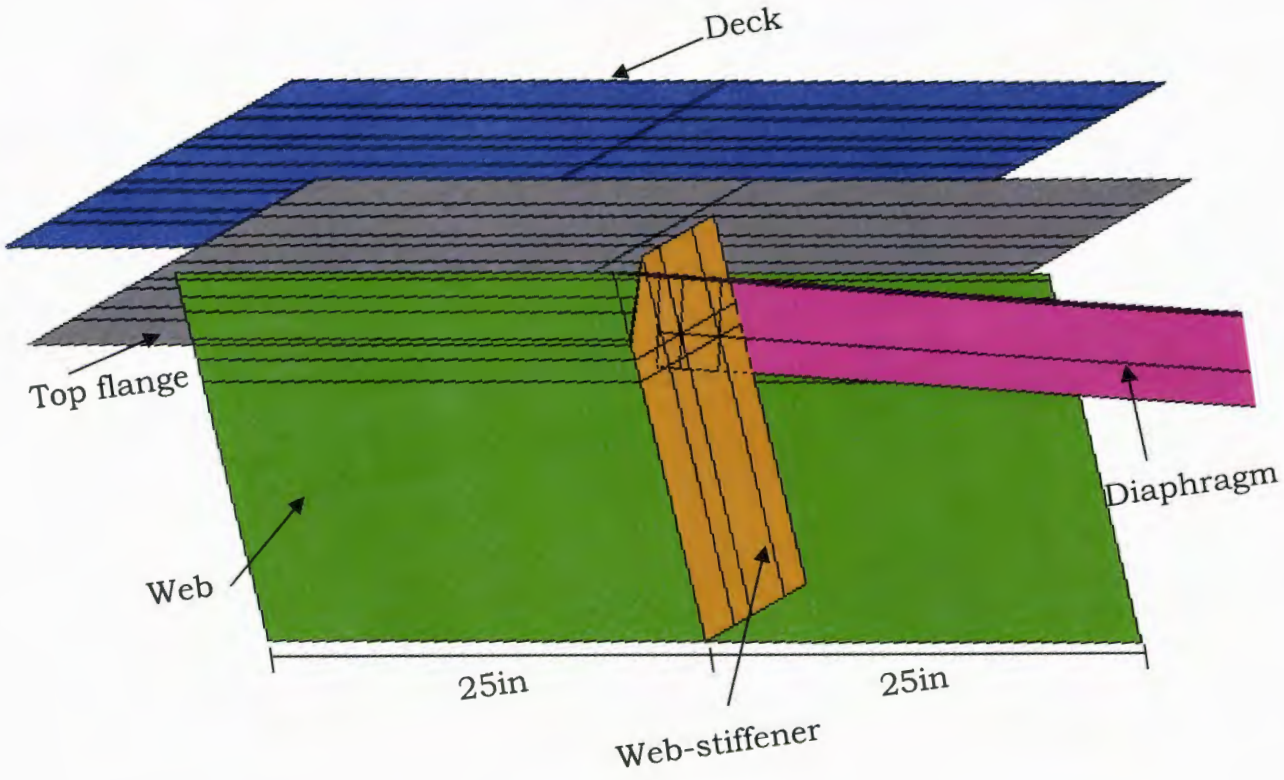

a. Side view of sub-model

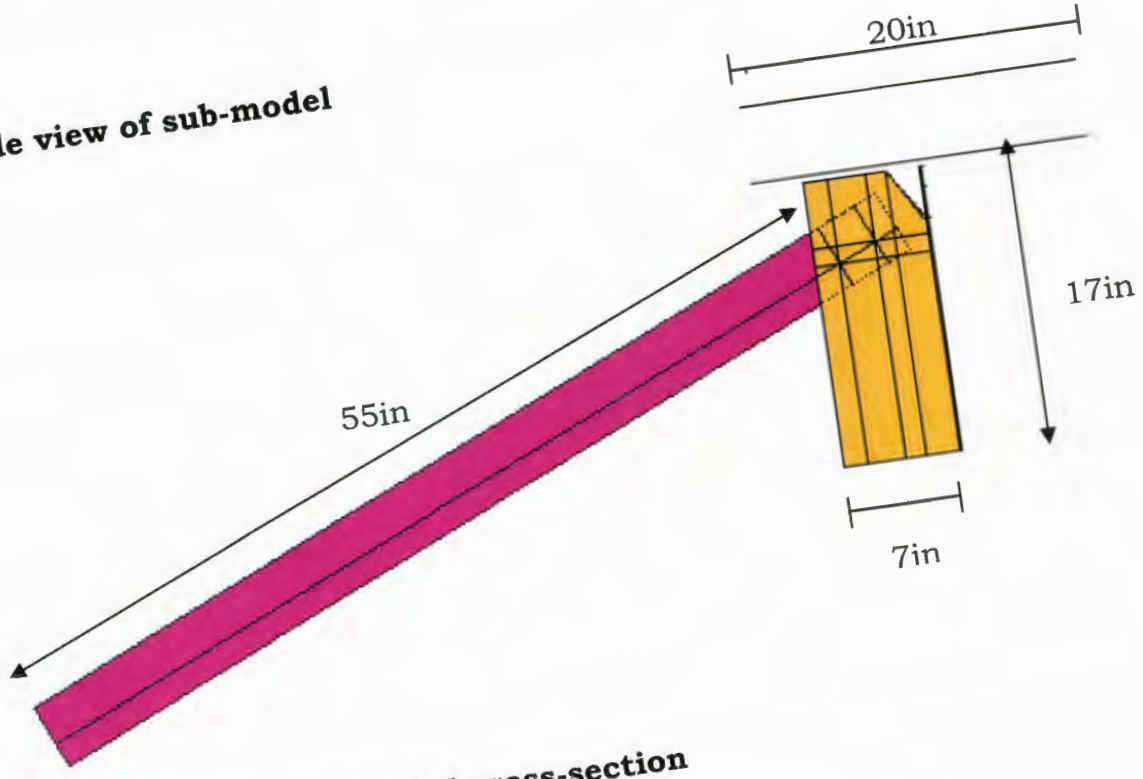

b. Front view of sub model cross-section

Figure 3.8 Different views of sub-model areas

corresponding to the web-stiffener and top of the girder were slave nodes. The deck nodes directly above the connection plate were linked with the girder nodes, the girder nodes being master nodes.

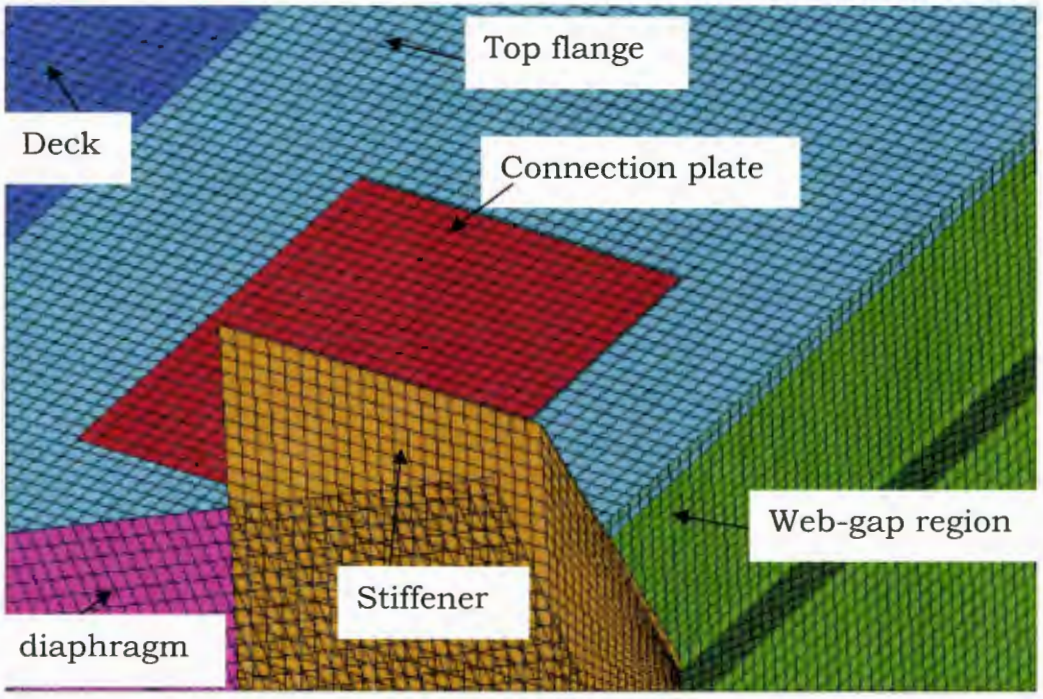

Figure 3.9 View of web-gap sub-model elements with connection plate

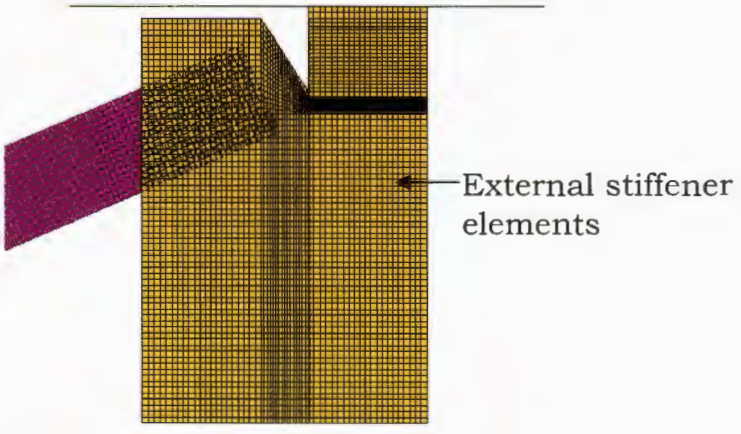

Figure 3.10 Sub-model elements with external stiffener

4. COMPARISON OF FINITE ELEMENT AND FIELD TEST RESULTS

4.1 Introduction

Calibration of a finite element analysis is an important step when analyzing complex structures. This can be accomplished by comparing obtained analytical results with those found from field, laboratory tests or in some cases, with published work. Such comparison is needed to verify the suitability of a finite element model and check the performance of the elements used in modeling the structure. This chapter presents the verification of the finite element model of the bridge structure that was detailed in the previous chapters.

As was mentioned previously in section 2.4, a total of eight load cases were considered during the field testing of the skewed bridge. Among these, four cases were considered for comparison with the results obtained from the finite element analysis. These were the load cases that were believed by the author of this study to represent the critical loading conditions on the bridge as they were expected to produce the maximum differential deflection between girders, and hence the maximum web-gap distortion.

4.2 Field measurements

4.2.1 Measured strains in the first web-gap from field test

The field test results of the strains in the web-gap region due to the load cases five, six, seven and eight whose truck load configurations were shown in section 2.4.2, are plotted in Figs.4.1 to 4.4. The figures summarize the variation in the vertical strains as the trucks traveled over the bridge deck. On these plots, strain-gage readings were denoted as g1, g2, g3, g4 and g5. The top and top strain-gages are represented by g1 and g5, respectively. As mentioned earlier, the top and bottom strain-gages were placed at 0.81 in. and 1.5 in. respectively, below the bottom of the top flange (see Fig. 2.15 for the locations of these gages). All the five strain-gages are placed within a height of 0.69 in. with equal spacing of about 0.17 in.

During the filed test, it was attempted to align the passes of the external wheels of the truck to be right over the external girder centerline for all load cases except in load cases four and eight, where the trucks were placed at the center of the lanes. However, some shifting of the truck load paths could easily take place since these alignments were visually done. The only information regarding the truck locations was provided by the two vertical marks. The first mark was taken when the front wheel of the truck reached the central pier (location 1) and the second, when it reached the web-gap location (location 2). A designation used on the plots shown in

Figs. 4.1 to 4.4 is referred to as 'm' and represents the two load positions (see Fig. 2.21). Also, the operator of the Data Acquisition System was informed to record these marks via a signal that was given to him by a person who was standing on the bridge deck and hence the location of the applied loads could not be precisely known.

The induced strains in the vertical direction of the girder web were recorded for about 25 seconds. Fig. 4.1 shows the strain recording at the five strain gage locations for load case five. The maximum tensile strain recorded was 11.58 $\mu\varepsilon$ at the location of the top strain gage, g1, and the maximum compressive strain recording was 11.82 $\mu\varepsilon$ for the bottom gage, g5. Similarly, the strain plots indicated that the top strain gages recorded the maximum tensile strains of 17.89 $\mu\varepsilon$ and 7.36 $\mu\varepsilon$ and the bottom strain gage recorded the maximum compressive strains of 22.02 $\mu\varepsilon$ and13.77 $\mu\varepsilon$ for load cases six and seven, respectively (see Figs. 4.2 and 4.3). However, for load case eight, a maximum tensile strain of 5.28 $\mu\varepsilon$ and a maximum compressive strain of 9.39 $\mu\varepsilon$ were recorded at the bottom and top strain-gages, respectively (see Fig.4.4).

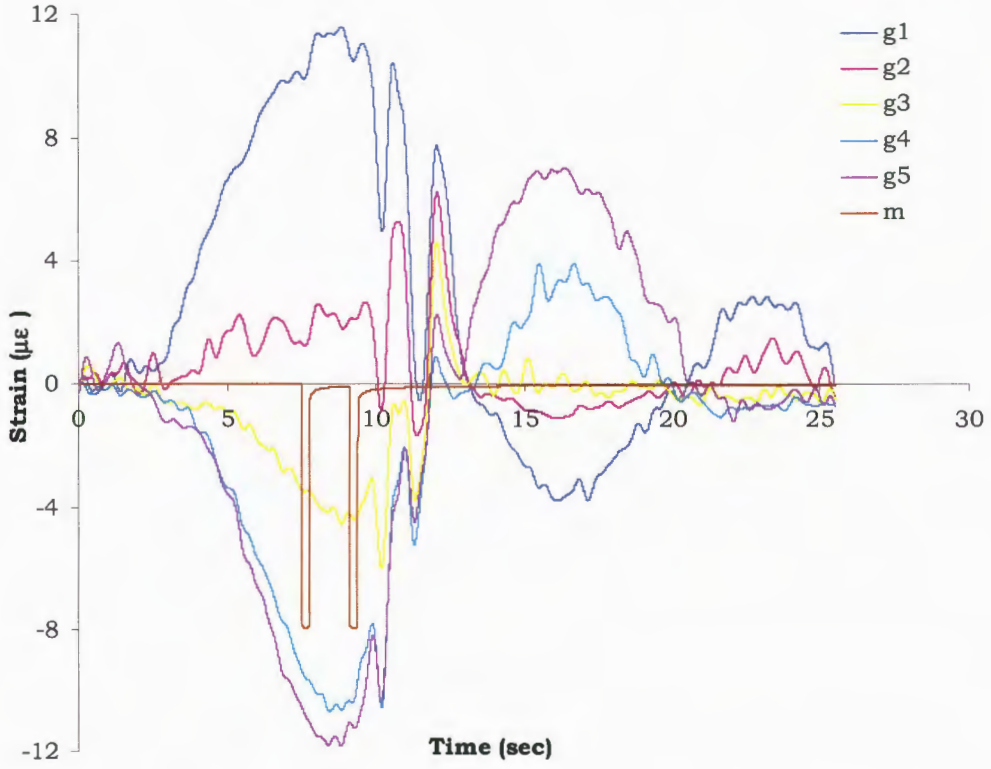

Figure 4.1 Measured vertical strains vs. time for load case five

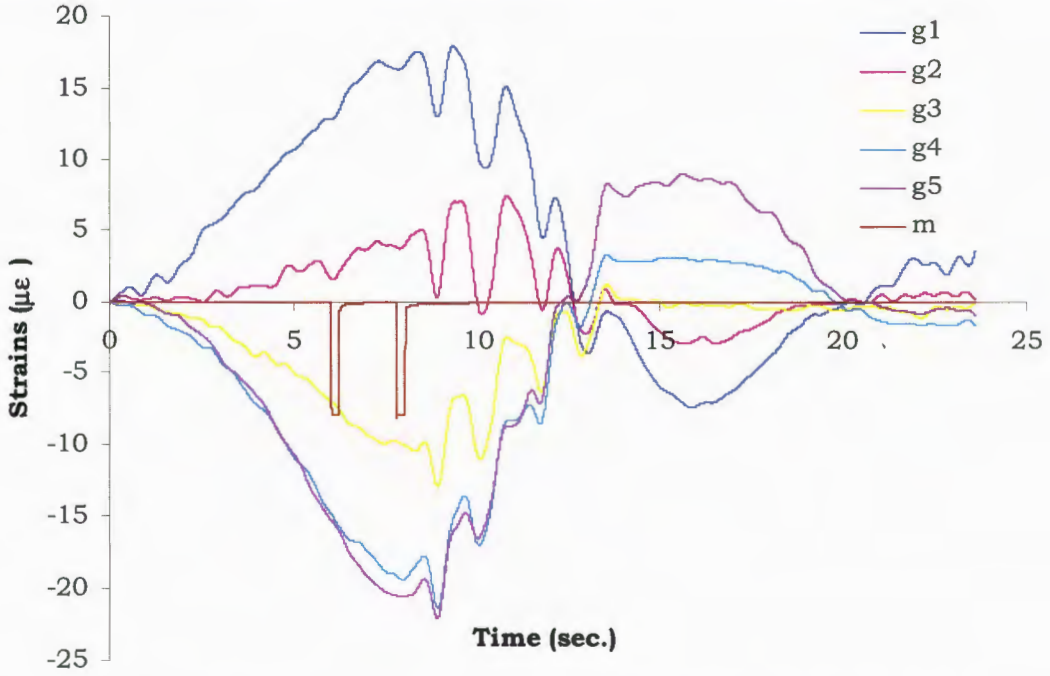

Figure 4.2 Measured vertical strains vs. time for load case six

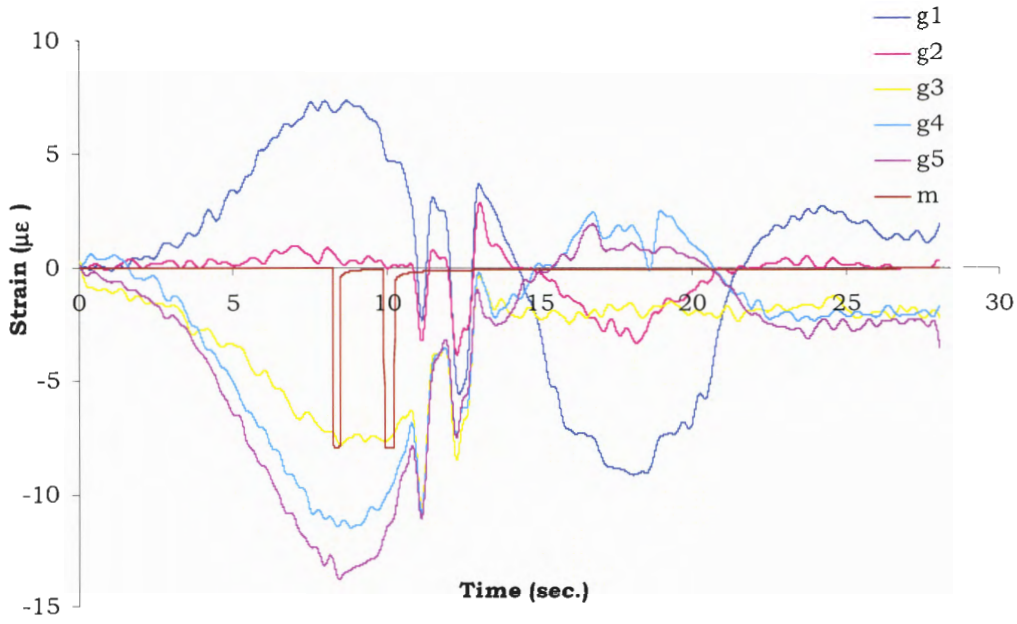

Figure 4.3 Measured vertical strains vs. time for load case seven

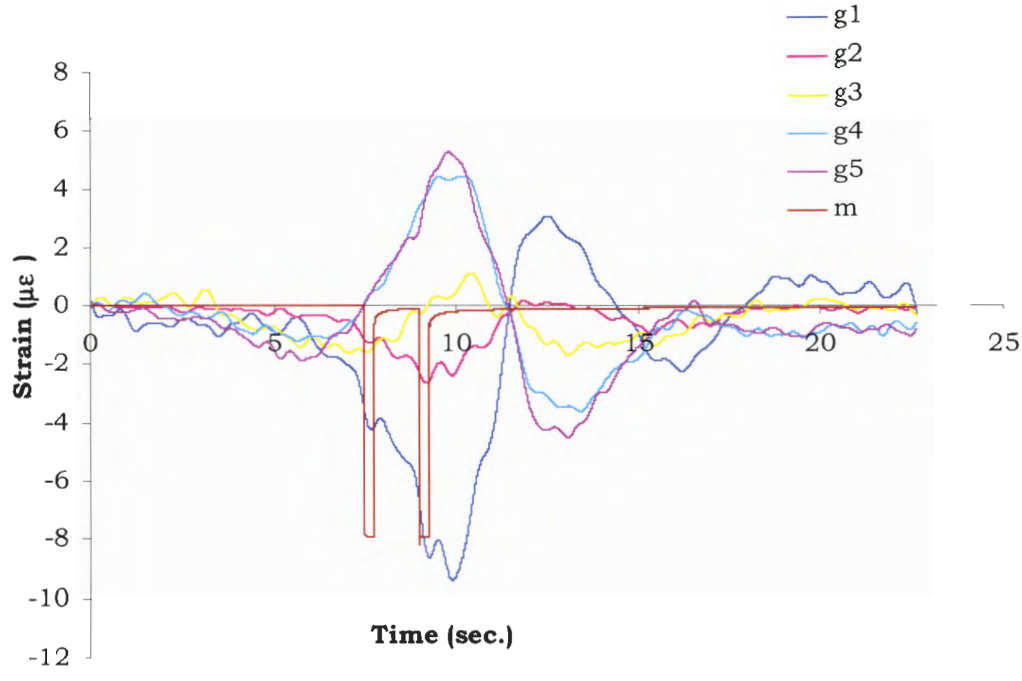

Figure 4.4 Measured vertical strains vs. time for load case eight

4.2.2 Strains in the diaphragm near the web-gap

As part of the field test, the strains that were induced at the three locations on the diaphragm (see Figs. 2.16 and 2.17) as the truck moved along the bridge deck were also recorded. Figures 4.5 through 4.8 summarize the strain variations in these gages as the truck loads traveled across the bridge. In addition, summarized in Table 4.1, are the recorded strains due to the four load cases when the front wheel of truck was placed directly above the web-gap (location 2).

The negative strains shown Table 4.1 indicate that the cross bracing of the diaphragm sustained compressive forces under load case 5, 6 and 7. On the other hand, for load case eight, positive strain readings of the three strain-gages on the cross bracing indicated that tensile forces were induced.

Table 4.1 Recorded strains in the cross-bracing near the web-gap

Load Cases	Top strain-gage ($\mu\varepsilon$)	Middle strain-gage ($\mu\varepsilon$)	Bottom strain-gage ($\mu\varepsilon$)
Load case five	-32.38	-72.10	-63.06
Load case six	-54.12	-119.16	-103.21
Load case seven	-25.79	-57.56	-49.85
Load case eight	15.64	33.29	31.53

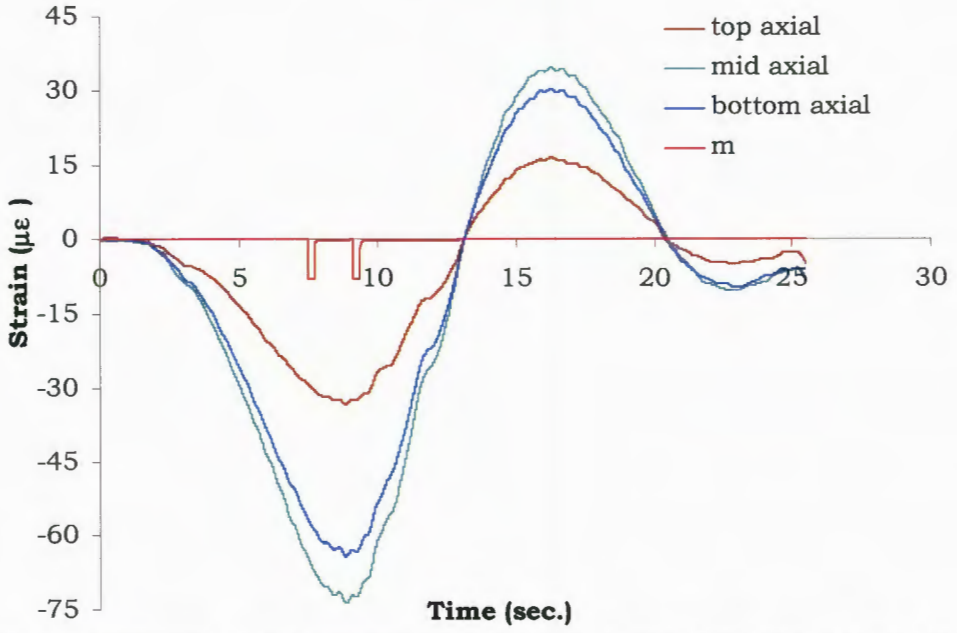

Figure 4.5 Measured diaphragm strains vs. time for load case five

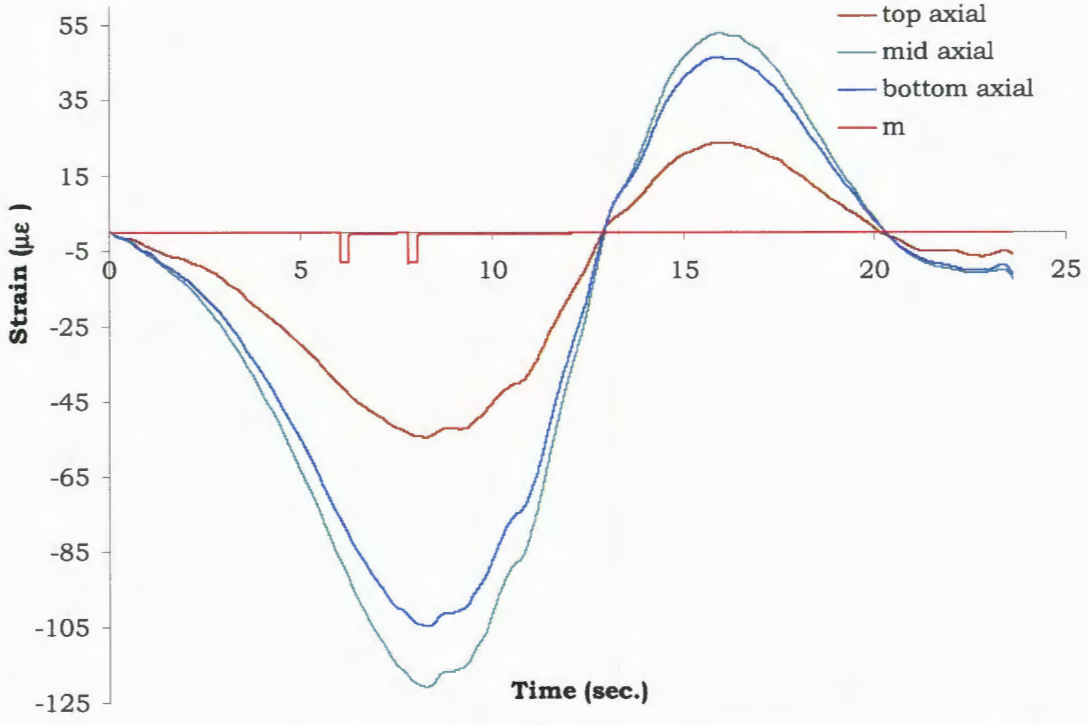

Figure 4.6 Measured diaphragm strains vs. time for load case six

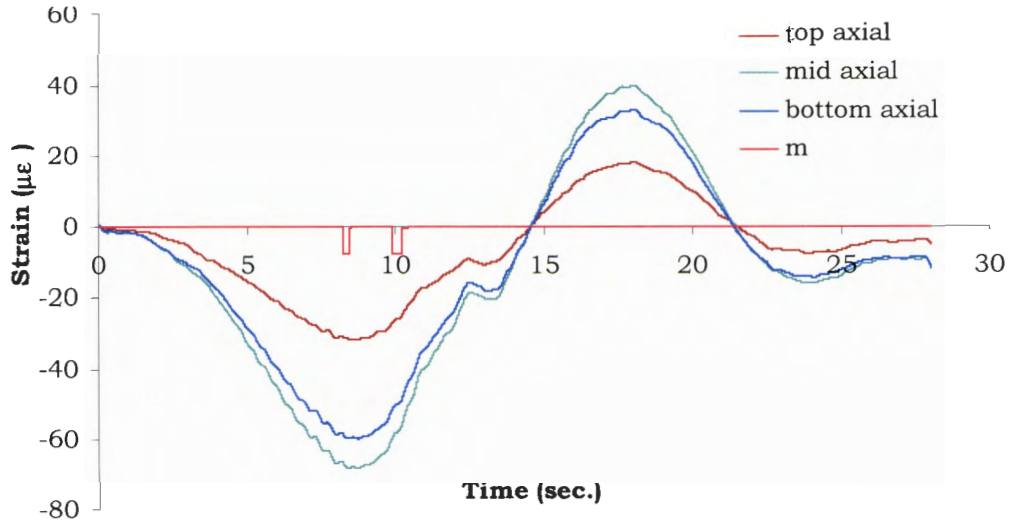

Figure 4.7 Measured diaphragm strains vs. time for load case seven

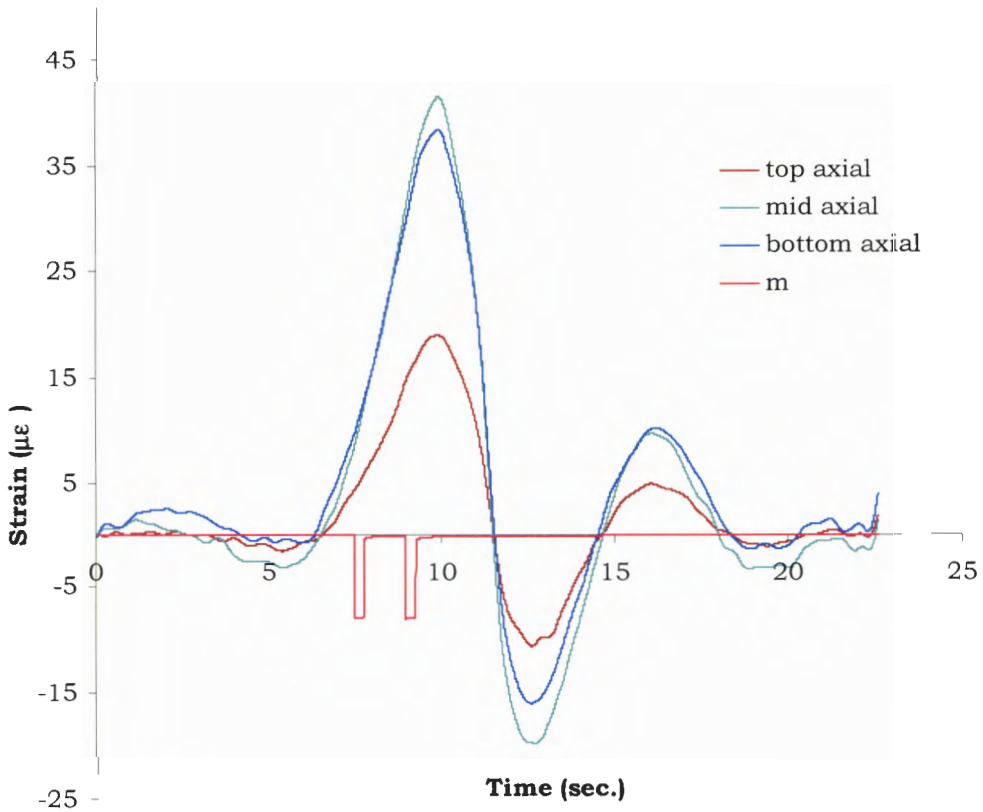

Figure 4.8 Measured diaphragm strains vs. time for load case eight

4.3 Comparison between finite element and field test results

As was mentioned before, the exact locations of the trucks on the bridge deck during the field tests were not recorded except for the positions that corresponded to the two tick marks as shown on the recorded strains. Therefore, these were the two locations that were used to position the loads on the bridge model utilized in the finite element analysis for verification with the field results. The strains that corresponded to these two locations were retrieved from Figs. 4.1 to 4.4 and were compared to those obtained from the analytical investigations. The results of these comparisons are summarized in Figs 4.9 to 4.12.

As can be seen from the these figures, the strains obtained from the finite element analyses showed some variations compared with those from the field test, mainly when the truck was positioned with the front wheels at location 2. The discrepancies between the field test and finite element results were even more pronounced for the two top gages. On the contrary, the finite element analysis yielded results that were in close agreement with the measured strains for the case where the front axle of the truck was positioned at location 1, especially for load cases five and six. These differences could have resulted from the sensitive nature of web-gap distortion to the load position, especially when the load was applied near the web-gap. In addition, these could have also resulted from accuracy limits of

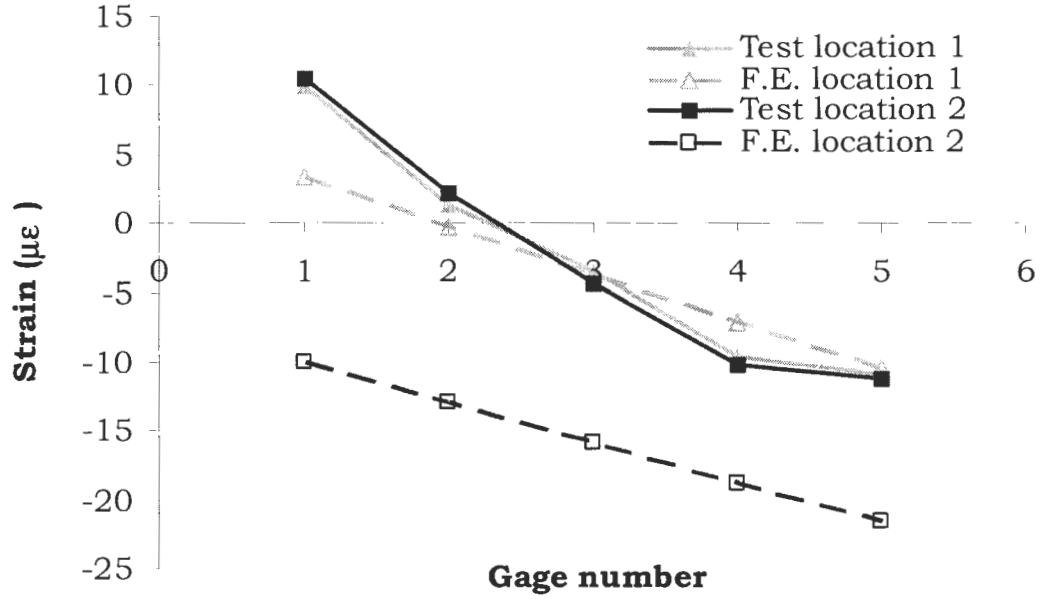

Figure 4.9 Measured vs. finite element results- load case five-Truck at locations 1 and 2

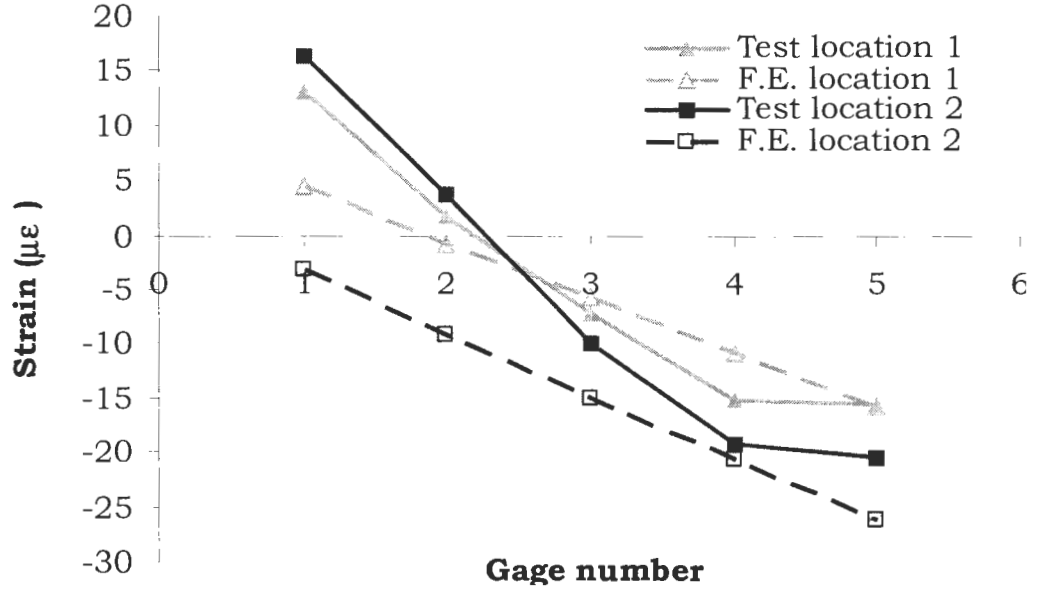

Figure 4.10 Measured vs. finite element results- load case six-Truck at locations 1and 2

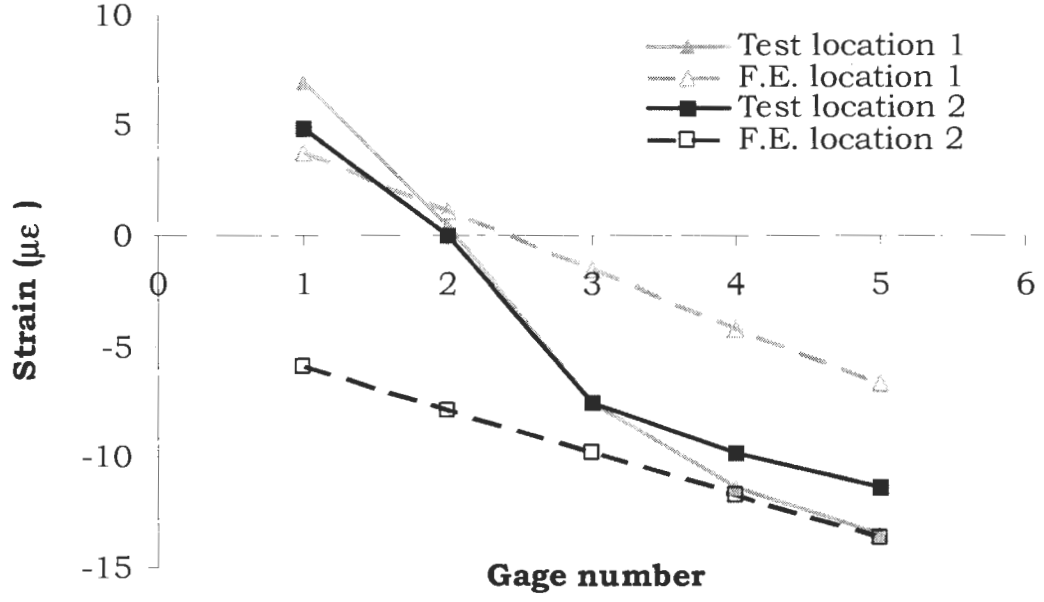

Figure 4.11 Measured vs. finite element results- load case seven-Truck at locations 1and 2

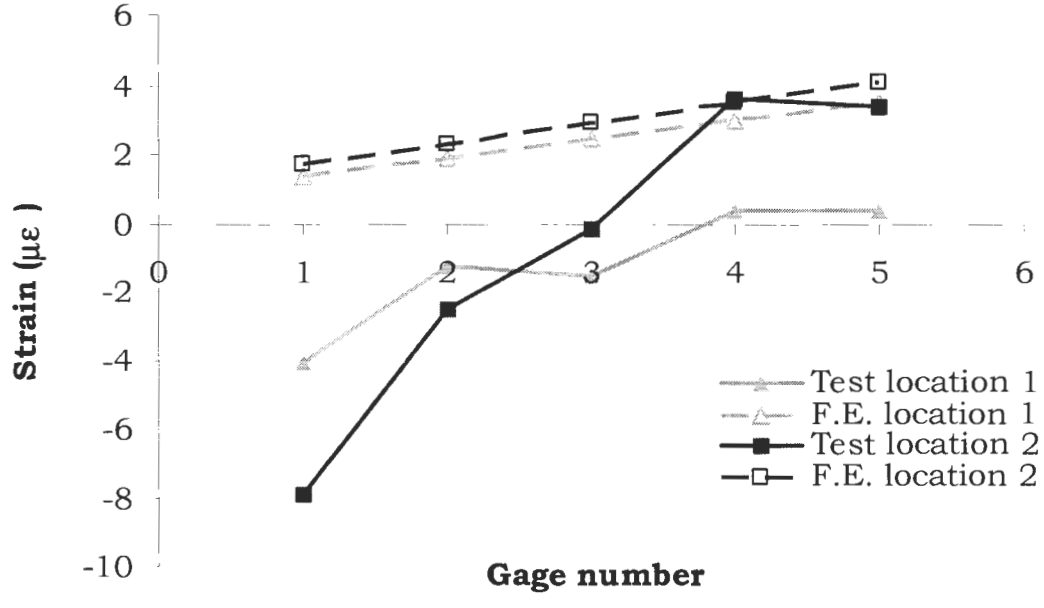

Figure 4.12 Measured vs. finite element results- load case eight-Truck at locations 1and 2

the instruments used in the field test or from not knowing the precise locations of the truck wheel loads and strain gauges. The effects of some of these factors were further investigated and the findings are discussed in the following chapter.

In light of the many possible factors that might have contributed to such discrepancies, it was decided that the margin of difference that occurred between the finite element results and the field measurements were acceptable. Hence, the finite element model was considered to be satisfactory to study the effect of other retrofit alternatives that can be used to minimize the out-of-plane distortion of the web-gap region in steel girder bridges.

5. ANALYSIS RESULTS FOR RETROFIT METHODS AND FACTORS AFFECTING WEB-GAP DISTORTION IN STEEL BRIDGES

5.1 Introduction

In this chapter, factors that affect the out-of-plane distortion induced in the web-gap region were studied. This was accomplished using the finite element model of the bridge that was developed and verified in the previous chapter. The original coarse- and sub-models described in chapter three were modified to include two repair methods that can be utilized to reduce the strains in the web-gap region. In addition, three more models were developed to investigate the effect of the height of the web-gap on the strains in this region.

First, the bridge was analyzed considering the structure without the plate connecting the stiffener to the top flange of the girder (referred to hereafter as no-retrofit). This case was used as a baseline and the results of it were compared with those obtained from analyzing the as-built bridge structure (referred to as retrofit A). Second, the impact of other retrofit methods such as loosening the bolts connecting the cross-bracing to the web-stiffener (retrofit B) or using additional stiffener on the opposite side of the web (retrofit C) on reducing the strains in the web-gap region were investigated. Third, using the modified finite element models that represent the varying web-gap heights, the behavior of web-gap distortion as a

function of web-gap height was studied. Finally, influence surfaces that represent the strains in the web-gap region as a unit load moves across the bridge structure were developed. These can be used to estimate the variation or the range of the strains induced in the web-gap region under different truck loads. Details of the developed influence surfaces for various internal responses of the web-gap region are presented.

5.2 Analysis of the bridge structure with and without retrofit

In this section, the results of analyzing the bridge structure with no retrofit and retrofit A are presented. This was carried out to investigate the effects of such a retrofit on the strains in the web-gap. In addition, the analysis results of the bridge with the assumed case of no retrofit was considered as a basis for investigating the effects of the different retrofit alternatives listed above on reducing the distortion induced in the web-gap region.

Fig.5.1 summarizes the results of the strains in the vertical direction that were induced in the web-gap region of the bridge in conjunction with no-retrofit and retrofit A. The strains at the locations that correspond to the locations of the strain gages used in the field test are presented in the figure. These locations are designated as nodes on the abscissa in the following figures. In these figures, node number 1 refers to the location of

the top stain gage while node number 5 corresponds to the location of the bottom gage. The stiffener and opposite-to-stiffener sides are shown by s and o, respectively.

As shown in Fig. 5.1, a maximum vertical strain of 274.86 μ was induced on the stiffener side in the case of no-retrofit, whereas the as-built case (retrofit A) resulted in a -9.98 μ. On the non-stiffener side, larger compressive strains were sustained by the case of no-retrofit. These results indicate that the web-gap was subjected to out-of-plane bending whose effect was diminished by the presence of the connection plate. This was due to the contribution of the connecting plate in the load transfer mechanism of the diaphragm force. Using such a connecting plate transfers the force in the cross-bracing directly to the top flange of the girder and hence reduces the distortion of the web-gap.

The finite element results of the principal strains on the side and the opposite side of the stiffener at the five gage locations, considering the cases with no retrofit and retrofit A, are shown in Fig. 5.2. As can be seen, the introduction of the connecting plate as a retrofit method resulted in a significant reduction in the principal strains when compared with those considering the no-retrofit case.

As previously mentioned the strain gages were located at 0.75 in. to the right of the stiffener. However, the finite element results did not indicate that these locations represented the location where the maximum strains occurred. On the contrary, the finite element analysis showed that maximum strains occurred at the stiffener tip and at the bottom of the weld joining the web to the girder top flange. The distribution of the vertical strains that occurred in the web-gap at these locations for the as-built bridge with no-retrofit and retrofit A is shown in Fig.5.3. This figure illustrates that the web-gap was subjected to out-of-plane bending, and the provision of connecting the stiffener and top-flange of the girder had considerably reduced this effect.

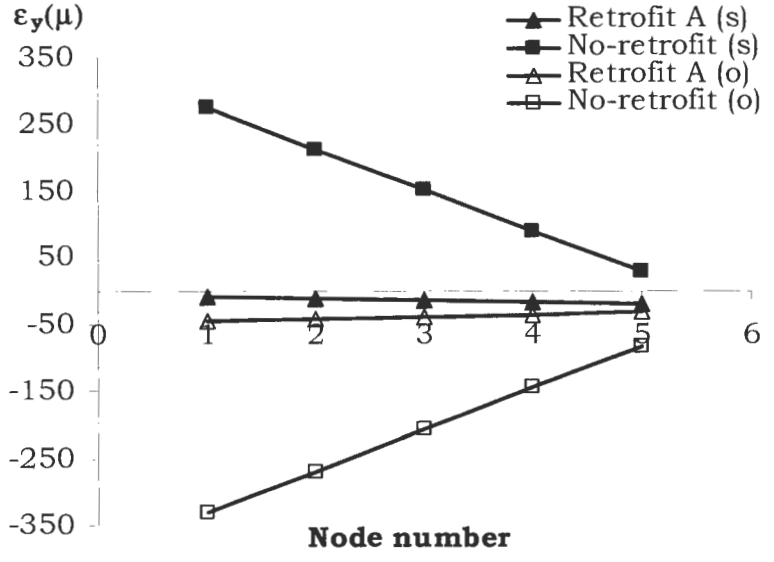

Fig.5.1 Distribution of vertical strain in the web-gap (no-retrofit and retrofit A)

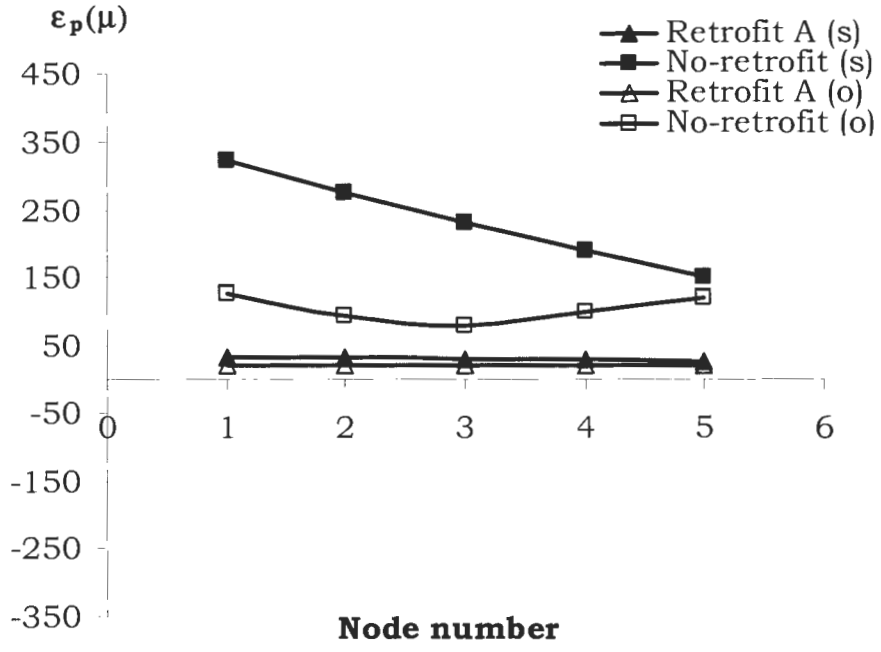

Fig.5.2 Distribution of principal strain in the web-gap (no-retrofit and retrofit A)

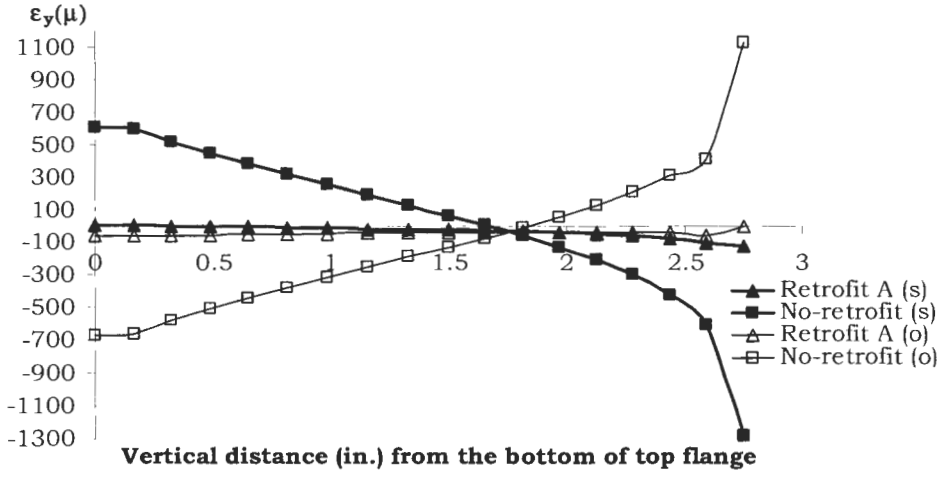

Fig.5.3 Distribution of vertical strain at critical location (no-retrofit and retrofit A)

5.3 Alternative retrofit methods

This section summarizes the results of analyzing the bridge structure considering plate connection of the web-stiffener to the top flange (retrofit A), loosening the bolts connecting the cross-bracing to the web-stiffener (retrofit B) and using additional stiffener on the opposite side of the web (retrofit C) on reducing the strains in the web-gap region.

Fig. 5.4 shows vertical strains for the various retrofits considered at the critical locations mentioned before. The results from the analysis of the no-retrofit case are also included in Fig.5.4. These results will be used to compare the retrofit methods and select the best alternative for the reduction of induced fatigue-stress in the web-gap region in similar bridge types.

The induced vertical strains in the web-gap region when retrofit alternatives A and B were used were found to be significantly lowered when compared with the no-retrofit case. On the stiffener side of the web-gap, the web-gap with no retrofit was subjected to a maximum strain of 608.78 μ right below the weld joining the web to the flange. This value was almost zero when the bridge was provided with either retrofit alternative A or B. On the other hand, the result showed only a 22% reduction of this strain when retrofit C was introduced. One may notice from Fig. 5.4 that aside from the

hot spots which were the stiffener tip and bottom of the weld mentioned above, the strains induced in the external stiffener retrofit alternative were concordant with the other two retrofits.

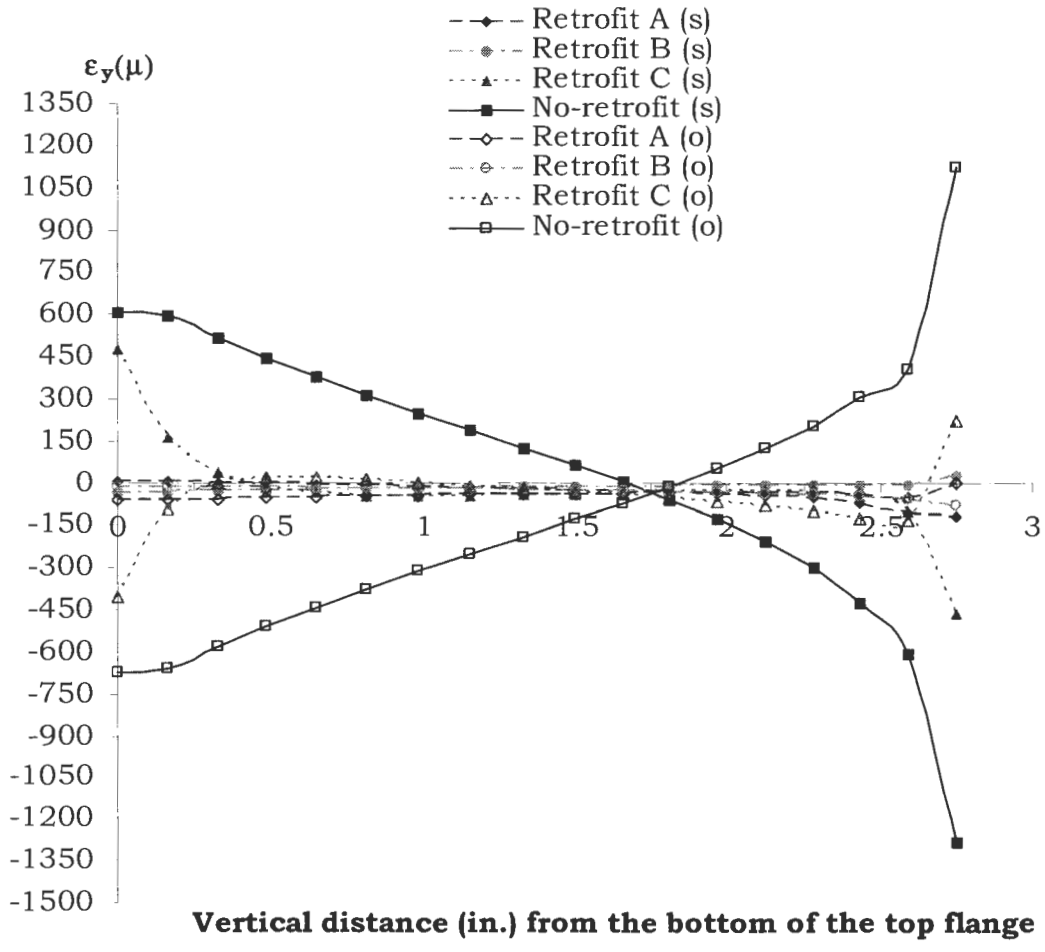

Fig.5.4 Comparison of vertical distribution of vertical strains in the critical region for different retrofit methods

The retrofit alternatives were also compared with respect to the vertical stresses induced at the critical locations in the web-gap region. These results are shown in Table 5.1. It can be noted from Table 5.1 that retrofit A and retrofit B were again found to have been almost fully effective in reducing the critical vertical stress that would have been induced for the no-retrofit case. Retrofit C was not found to be as effective as the two other retrofits yielding a 31.5% reduction in the vertical stress for the top critical node on the stiffener side. The vertical stress contour plots for the stiffener and opposite to stiffener sides for the no-retrofit case are shown in Fig. 5.5. Note the vertical stress hot spots at the critical locations in the web-gap at the stiffener-web weld in Fig.5.5.

Table 5.1 Vertical stress comparison for different retrofit alternatives

	Top critical vertical stress(ksi)		Bottom critical vertical stress(ksi)	
Retrofit Cases	Stiffener side	Opposite to stiffener side	Stiffener side	Opposite to stiffener side
No-retrofit	20.14	-21.97	-52.44	47.77
Retrofit A	-0.13	-0.86	-4.25	0.63
Retrofit B	-1.06	-0.37	1.32	-2.90
Retrofit C	13.78	-11.58	-17.46	10.40

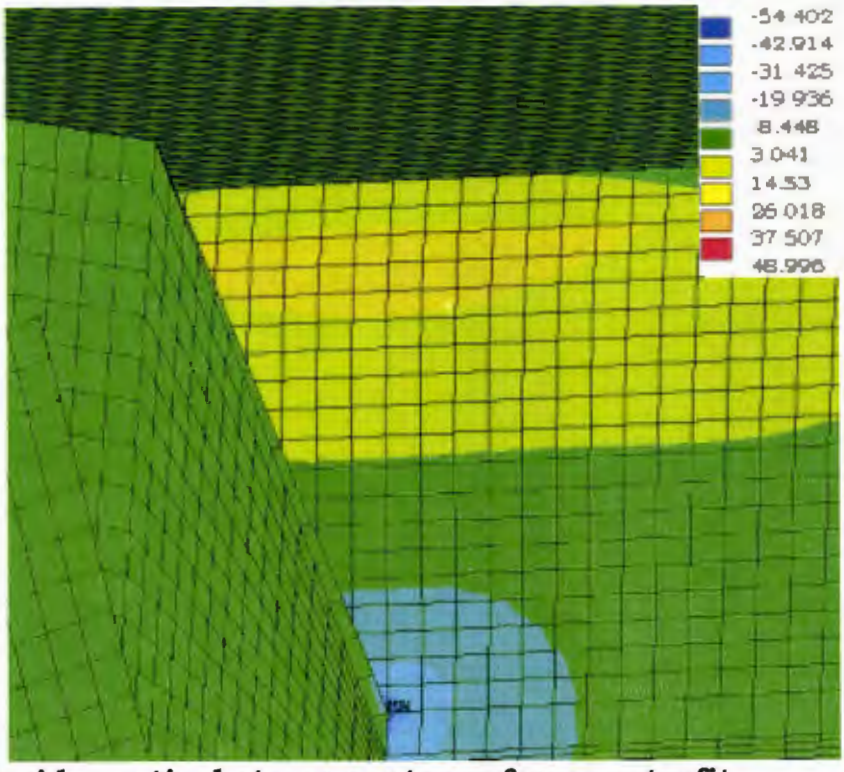

a. Stiffener side vertical stress contours for no-retrofit

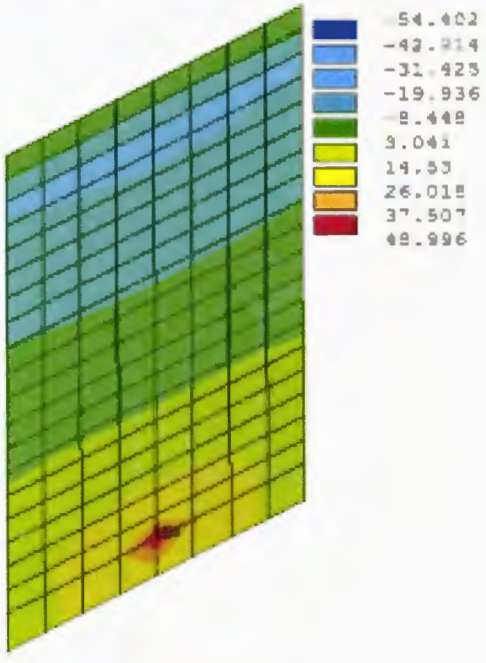

b. Opposite-to-stiffener side vertical stress contours for no-retrofit

Fig.5.5 Vertical stress contours for no-retrofit

5.4 Study of the effect of web-gap height on out-of-plane distortion of the web-gap region

In this section the effect of the height of the web-gap on the out-of-plane distortion is summarized. This was carried out based on the recommendation in Ref. [8]. For the comparison three different heights of 2.6 in., 2.75 in. and 3 in. were considered.

Comparison of the vertical strains is shown in Fig.5.6. The results in the figure indicate that, on the stiffener side of the top gage location, the shorter gap sustained a slightly higher strain, followed by the medium and long web-gap heights. Similarly, on the opposite-to-stiffener side, the web-gap heights were inversely related to the induced vertical strains. This was more significantly so at the bottom gage location.

Figure 5.7 shows a comparison between the principal strains induced on the stiffener and opposite-to-stiffener sides at the five strain gage locations. In both cases, the shortest web-gap resulted in the maximum principal strains whereas the longest web-gap resulted in the minimum principal strains.

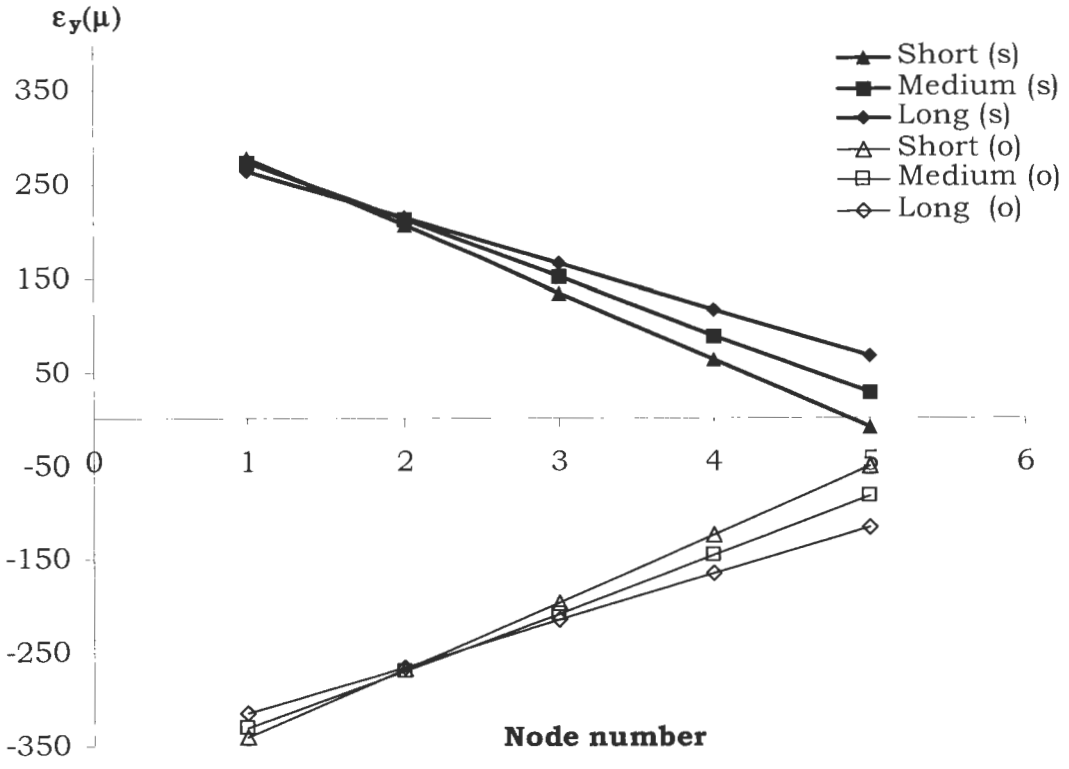

Fig. 5.6 Vertical strain comparisons for the different web-gap heights

To investigate the effect of web-gap height variation on the out-of-plane distortion in the critical region directly above the stiffener, the vertical distribution of the vertical strains were plotted for the three web-gap heights. The plots of the strain distribution in the critical web-gap region for these web-gap height variations are shown in Fig.5.8.

The short web-gap resulted in a maximum strain of 669.14 μ and 1383.2 μ on the stiffener and opposite-to-stiffener sides respectively. Maximum vertical strains of 608.78 μ and 1123.2 μ were found on the

stiffener and non-stiffener sides for the medium web-gap. Correspondingly, the stiffener and non-stiffener sides of the long web-gap yielded maximum strains of 527.78 μ and 902.52 μ respectively. The vertical strain results showed that the short web-gap exhibited increments of 27% and 53.26% on the stiffener and opposite-to-stiffener sides, respectively, when compared to the long web-gap height, approximately 2/5 inches longer.

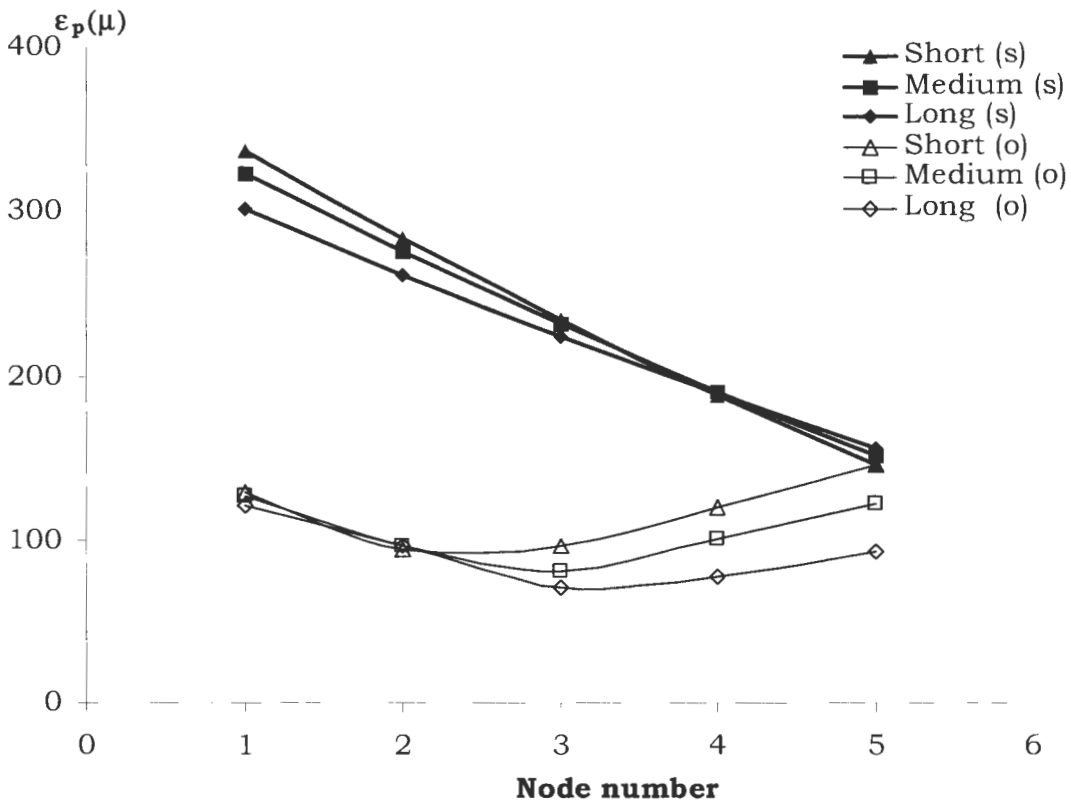

Fig.5.7 Comparison of principal strains for the different web-gap heights

In the case of shorter web-gap heights, the increase in strains obtained from the finite element analysis indicate that the web-gap distortion is considerably affected by the stiffness of the web-gap. The shorter the web-gap height, the relative out-of-plane displacement induced by the diaphragm forces result in higher bending effects due to the fact that the flange adjacent to the top of the web-gap is imbedded in the rigid deck.

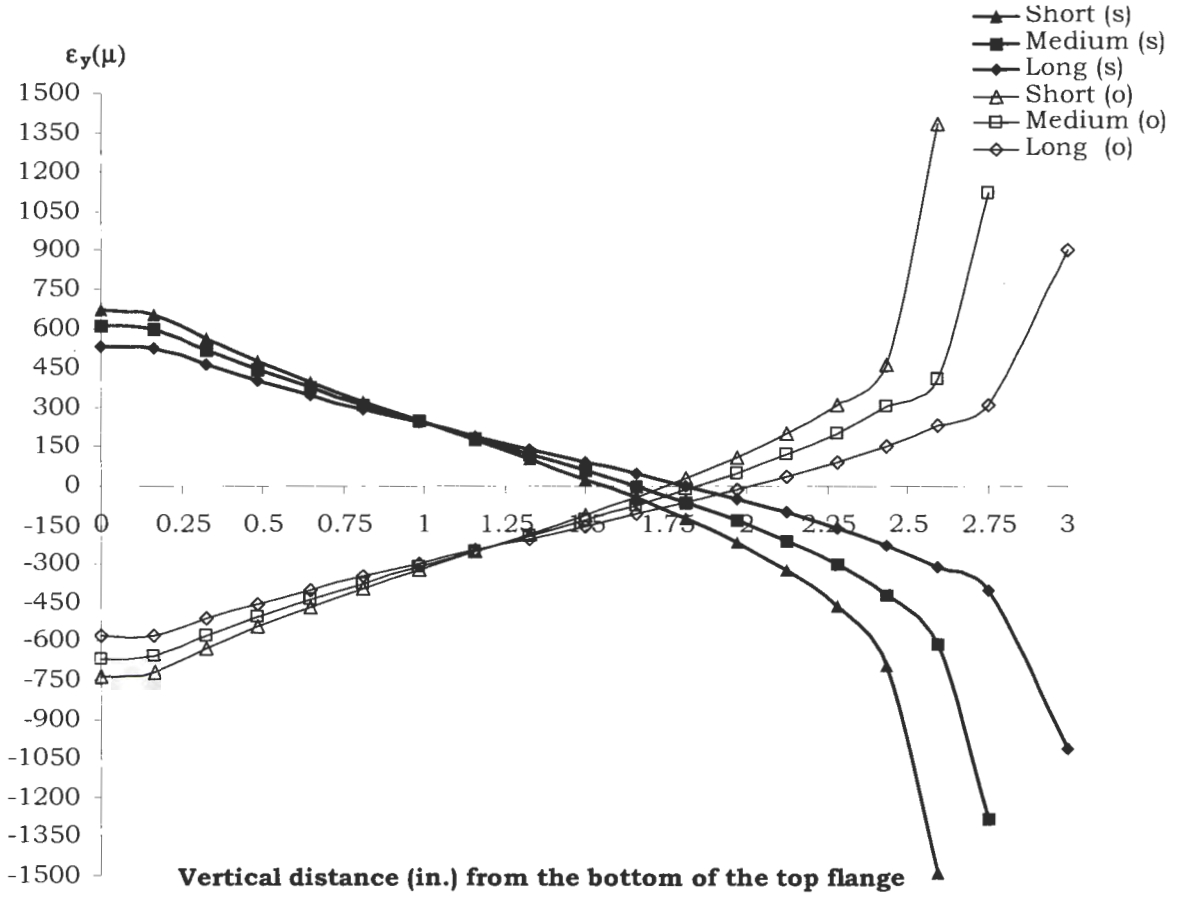

Fig.5.8 Comparison of vertical distribution of vertical strains for the different web-gap heights at the critical location

5.5 Influence surfaces

The behavior of web-gap distortion is a complex phenomenon that requires detailed analysis. In order to simplify such a task, several finite element analyses for the no-retrofit case of the bridge structure were carried out and the results were employed to develop influence surfaces that one can utilize to investigate the behavior of the web-gap region of similar bridge types. In this section, discussions on developing and interpreting influence surfaces for induced strains, out-of-plane displacement in the web-gap, and the force in the adjacent diaphragm with respect to varying load positions on the bridge are presented.

5.5.1 Influence surface for strains

The first step of the development of influence surfaces of internal responses in the web-gap region of the multi-girder steel bridge was to decide on the number of loading points to consider. Previous analysis results indicated that the internal responses could be significantly affected for the wheel load positions closer to the web-gap region near the central pier. For this reason, it was decided to select the loading points to be close to each other in the vicinity of the web-gap region near the central pier, and spread apart as one moves away from the central pier towards the exterior piers. On the other hand, the transverse distance between the loading points was maintained as 55.5 in. A total of 9 loading points were

considered across the bridge width. This resulted in the use of a total of 153 loading points to develop the influence surfaces for the structural responses of the web-gap.

The coordinate system used in the subsequent analyses of influence surfaces has its origin at the centre of the central pier. The x- and y- axes refer to the longitudinal and transverse directions on the bridge, respectively.

5.5.1.1 Influence strain surfaces at tested nodes

To further verify the analytical results and to investigate the effects of the load position on the calculated strains, influence surfaces for strains at the top and bottom strain gages were first developed. This was accomplished by analyzing the bridge structure considering a unit load that was positioned at various locations on the bridge deck.

The choice of the number of points to include for fitting of the polynomial regression equation depended on the accuracy desired. The desired accuracy was found to be improved when a reasonable number of data points were included in the regression analysis. This was due to considerable variation of the finite element results in particular when the distance between the data points was increased. For this reason, each of

the two spans of the bridge that were included in the finite element model was divided into three sections. For each span, the first section ran from the central pier to 235.5 in; the second and third sections ran from 235.5 in. to 768 in. and 768 in. to 1300.5 in., respectively.

The first section which runs from the central pier to 235.5 inches in the west direction was selected for investigation. There were a total of 27 data points of strain verses coordinate location. This section was chosen since it included data points that were close to the central pier which were found to be critical loading points as to their impact on the behavior of web-gap distortion.

The results of the loading points considered were utilized to estimate the coefficients of the polynomial equation listed below to estimate the vertical strain at the locations of the two strain-gages:

$$\varepsilon_y = A + Bx^0y^1 + Cx^0y^2 + Dx^0y^3 + Ex^0y^4 + Fx^0y^5 + Gx^1y^0 + Hx^1y^1 + Ix^1y^2 + Jx^1y^3 + Kx^1y^4 + Lx^1y^5 + Mx^2y^0 + Nx^2y^1 + Ox^2y^2 + Px^2y^3 + Qx^2y^4 + Rx^2y^5 \quad \text{..(5-1)}$$

where:

ε_y = Vertical strain

$A, B, C.....R$ = Coefficients

x, y = Coordinate of the location where the load is applied

Four equations representing the influence surface for the strains at the top and bottom gage locations on both sides of the girder web (see section 2.3.1 for the locations of these gages) were developed. The coefficients of the polynomial relationship given in Equation 5-1 for each of these cases are listed in Table 5.2.

The accuracy of the developed equations for these strains was checked. This was accomplished by comparing the results obtained from the direct finite element analysis of the bridge structure under load case five with those obtained using the developed equations. For this purpose the strains at the locations of the top and bottom gages in conjunction with the no-retrofit and retrofit A cases were utilized when one of the front wheels of the truck was directly above the web-gap (previously designated as position m 2(location 2)). The dimensions of the truck shown in Fig.2.19 were used to position the rest of the truck wheels on the bridge deck. The strains that were induced at the top and bottom gage locations due each wheel load were then calculated and algebraically added to estimate the total strains that were caused by the truck.

A summary of the strains estimated using the developed equation and finite element results is given in Tables 5.3. The table shows the close agreement between the results obtained using these two approaches. This

Table 5.2 Coefficients of strain influence surface equation for tested locations

Coefficients	Bottom on stiffener side	Bottom opposite-to-stiffener side	Bottom on stiffener side	Top opposite-to-stiffener side
A	-3.98E-11	4.45E-11	-1.41E-10	1.41E-10
B	1.66E-09	4.15E-10	-2.05E-08	2.23E-08
C	-3.31E-11	5.12E-11	-1.13E-10	1.33E-10
D	-4.81E-13	3.95E-13	4.97E-14	-1.09E-13
E	6.10E-16	-2.18E-15	4.66E-15	-6.30E-15
F	7.64E-18	-1.18E-17	1.13E-17	-1.61E-17
G	-3.13E-09	3.49E-09	-1.10E-08	1.10E-08
H	-5.59E-11	3.33E-11	-1.36E-10	1.23E-10
I	5.75E-13	-7.92E-13	1.92E-12	-2.13E-12
J	5.31E-15	-3.96E-15	1.48E-14	-1.42E-14
K	-6.84E-18	2.55E-17	-3.99E-17	5.89E-17
L	-2.44E-20	6.84E-20	-1.24E-19	1.83E-19
M	7.20E-12	-7.78E-12	1.50E-11	-1.40E-11
N	1.79E-13	-1.22E-13	8.19E-13	-7.96E-13
O	-1.51E-15	2.04E-15	-4.10E-15	4.57E-15
P	-1.08E-17	6.25E-18	-4.68E-17	4.51E-17
Q	2.16E-20	-7.29E-20	9.83E-20	-1.50E-19
R	-5.04E-23	-5.91E-23	2.14E-22	-3.77E-22

indicated that the number of loading points considered in developing the coefficients in Equation 5-1 were sufficient to predict the strains in the web-gap.

Table 5.3 Summary of FE verses influence surface equation results

	$\varepsilon(\mu)$	
Location	FE	Influence Surface Equation
Bottom opposite-to-stiffener side	-82.59	-79.70
Bottom Stiffener side	27.48	31.72
Top opposite-to-stiffener side	-331.27	-330.1
Top Stiffener side	274.86	281.01

5.5.1.2 Influence strain surfaces at critical node locations

The Influence surfaces that were developed so far dealt with the strain response at a location where field test measurements were carried out, i.e. at a location of 0.75 inches offset from the stiffener. However, the nodes of the web-gap region elements directly above the stiffener and below the weld of the web-flange connection were the critical ones that needed further investigation. Hence, it was important to develop strain influence surfaces at these two critical nodes.

The stiffener and opposite-to-stiffener sides for each of these two critical nodes were considered. Using the polynomial regression equation, Equation 5-1, the coefficients of which are listed in Table 5.4, the strain influence surfaces were developed.

Verification of the accuracy of the four strain influence surfaces was accomplished by comparing the results of these equations for load case five (see Table 5.5) with the finite element results directly obtained through the direct application of load case five. These results show good agreement indicating that the strain influence equations were satisfactory to describe the strain response in the web-gap.

Plots of the strain influence surface magnified by 100 at the top critical node on the stiffener side are shown in Figs.5.9 & 5.10. The plots for the opposite-to-stiffener side at the bottom critical node magnified by 100 are shown in Figs. 5.11 & 5.12.

5.5.1.3 Impact of position of load on measured strains

The influence strain surfaces developed in the previous sections were utilized to investigate the impact of the position of the wheel load on the induced strains in the web-gap region in the multi-girder steel bridge that was studied herein.

Table 5.4 Coefficients of strain influence surface equation for critical locations

Coefficients	Bottom on stiffener side	Bottom opposite-to-stiffener side	Bottom on stiffener side	Top opposite-to-stiffener side
A	-2.45E-10	2.46E-10	5.66E-10	-4.79E-10
B	-4.79E-08	4.94E-08	1.09E-07	-9.97E-08
C	-2.20E-10	2.45E-10	3.79E-10	-3.34E-10
D	6.34E-13	-6.41E-13	-2.96E-12	2.65E-12
E	1.01E-14	-1.20E-14	-2.09E-14	1.75E-14
F	1.79E-17	-2.41E-17	-1.61E-17	9.78E-18
G	-1.92E-08	1.93E-08	4.44E-08	-3.76E-08
H	-3.05E-10	2.97E-10	3.58E-10	-4.07E-10
I	2.42E-12	-2.70E-12	-6.17E-12	4.23E-12
J	3.76E-14	-3.77E-14	-4.70E-14	5.38E-14
K	-3.42E-17	5.59E-17	1.47E-16	-6.72E-17
L	-5.49E-19	6.27E-19	6.61E-19	-8.08E-19
M	1.53E-11	-1.43E-11	-6.09E-11	4.18E-11
N	1.90E-12	-1.90E-12	-3.02E-12	3.08E-12
O	-2.05E-15	2.68E-15	1.09E-14	-4.17E-15
P	-1.36E-16	1.36E-16	1.85E-16	-2.13E-16
Q	-1.02E-20	-4.80E-20	-2.93E-19	1.25E-20
R	1.78E-21	-1.99E-21	-2.06E-21	2.83E-21

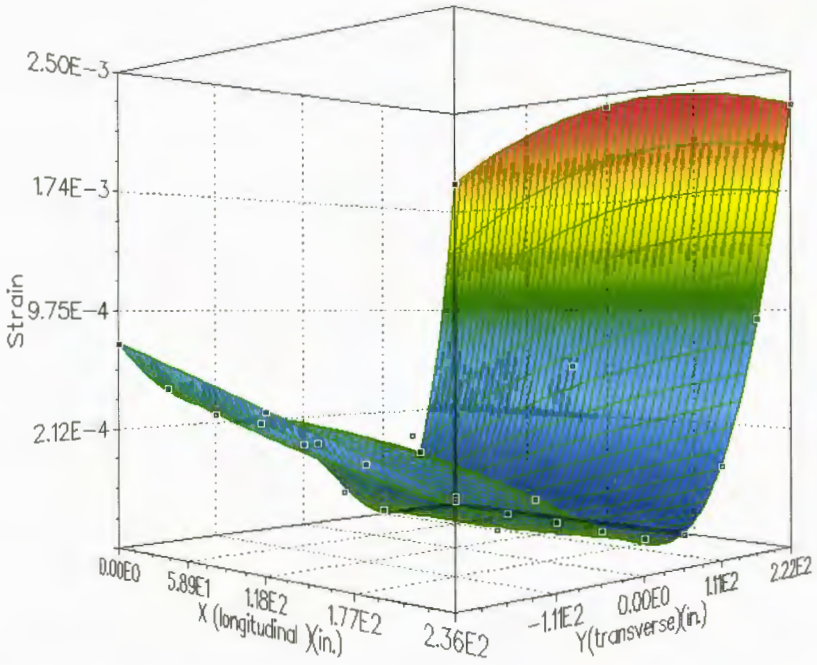

Fig.5.9 Three dimensional strain influence surface plot at stiffener side top critical location

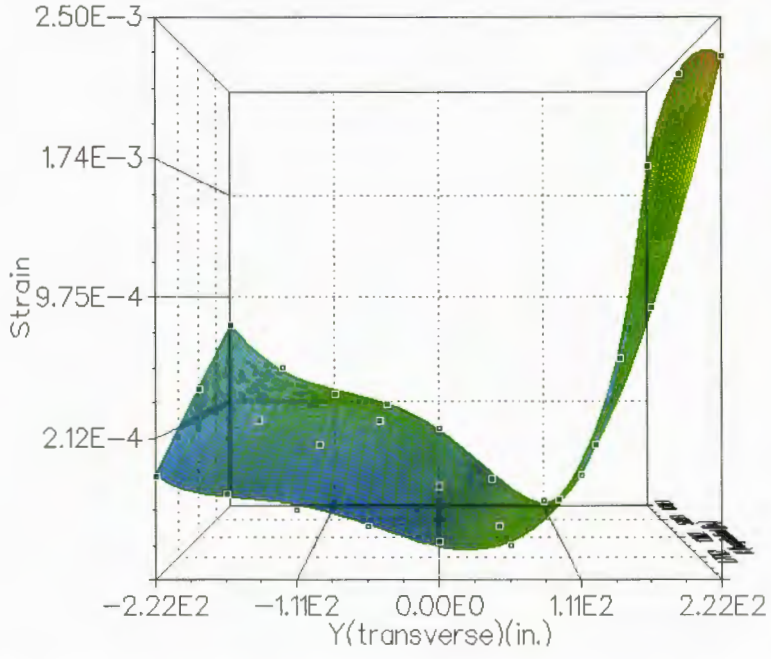

Fig.5.10 Front view of strain influence surface plot at stiffener side top critical Location

Table 5.5 Stiffener side strains using equation at the top critical location

	$\varepsilon(\mu)$	
Location	FE	Influence Surface Equation
Bottom opposite-to-stiffener side	1123.20	1136.24
Bottom Stiffener side	-1281.40	-1285.30
Top opposite-to-stiffener side	-669.51	-669.80
Top Stiffener side	608.78	618.62

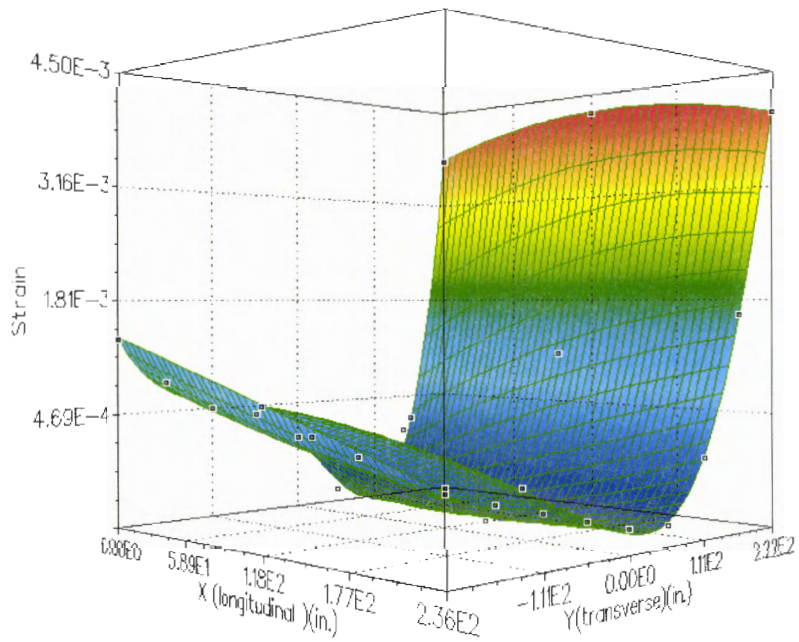

Fig.5.11 Three dimensional strain influence surface plot for opposite-to-stiffener side at the bottom critical location

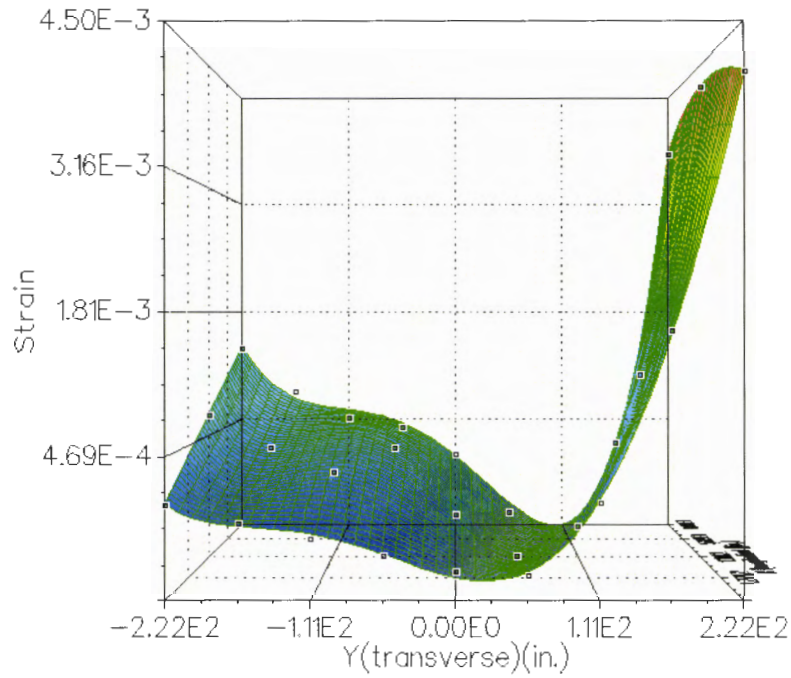

Fig.5.12 Front view of strain influence surface plot for opposite-to-stiffener side at the bottom critical location

Load case five was once again chosen for this study with the leftmost front wheel positioned at (x=0, y=vary) and (x=vary, y= 143.5 in.). Table 5.6 shows the variation of strain with wheel load position. As can be noticed, there is significant variation of strain with the slight change in loading position near the central pier. For the single truck considered, a difference of 1 ft in load positioning near the central pier resulted in an approximately 12 $\mu\varepsilon$ difference in induced strain. This effect would be even more pronounced in the case loading the bridge with two trucks. In this case, controlling the positions of the wheels of the trucks could be quite difficult during field testing and therefore, one should expect some differences between the test and finite element results.

Table 5.6 Variation of strain with wheel load position on the stiffener side

Leftmost wheel position (in.)		$\varepsilon(\mu)$	
x	y	Bottom	Top
0	122	11.54	153.53
0	131.75	19.48	206.00
0	133	20.62	213.26
0	143.75	31.72	281.01
12	143.75	34.64	287.09
24	143.75	36.47	292.70
48	143.75	36.93	296.47

The impact of wheel load positioning on the induced strains at the critical locations of the web-gap region was also investigated. This was done by positioning the leftmost front wheel at (x=0, y=vary) and (x=vary, y=111in.). The results of this investigation are summarized in Tables 5.7 & 5.8. As can be seen, the impact of variation in wheel load positioning is found to be of significance on the strains at the critical locations. Moreover, it can be noted that transverse variation in the position of the truck resulted in a considerable change in strain variation at the critical locations than similar variation in longitudinal position. Therefore it is recommended to carefully monitor the accurate locations of the truck

wheel loads when carrying out field test measurement of strains especially when comparing field test and analytical results.

Table 5.7 Transverse load position impact on strain at critical location

Leftmost wheel position (in.)		$\varepsilon(\mu)$	
x	y	Bottom	Top
0	0	288.89	-149.69
0	12	289.02	-153
0	24	274.82	-145.54
0	36	243.47	-131.79
0	48	192.1	-108.3
0	60	117.76	-73.51
0	72	17.47	-25.82
0	84	-111.72	36.37
0	96	-272.78	114.71
0	108	-468.61	210.83
0	120	-702.01	326.37
0	132	-975.72	462.96
0	143.75	-1285.28	618.62

Table 5.8 Longitudinal load position impact on strain at critical location

Leftmost wheel position (in.)		$\varepsilon(\mu)$	
x	y	Bottom	Top
0	111	-523.33	237.83
12	111	-549.99	254.52
24	111	-576.30	270.06
36	111	-602.24	284.45

5.5.2 Influence surface for diaphragm force

Influence surface was also developed to estimate the force in the cross bracing. This was accomplished using Equation 5.1, with the dependent variable vertical strain replaced by diaphragm force, and the coefficients from Table 5.9.

Plots of the diaphragm force influence surfaces magnified by 100 are shown in Figs. 5.13 & 5.14. The direct finite element analysis for the bridge with the front wheel of the truck positioned over the web-gap region for load case five was 2.016 kips and the estimated force using Equation 5-1 was 2.032 kips. This indicated that the adequacy of the developed relationship that can be used to estimate the force in the cross bracing of the diaphragm system.

Table 5.9 Coefficients of diaphragm influence surface equation

Coefficients		Coefficients	
A	-1.38E-04	J	5.12E-09
B	-1.75E-02	K	-1.88E-11
C	-7.33E-05	L	-9.18E-14
D	3.89E-07	M	2.50E-05
E	3.50E-09	N	2.17E-07
F	4.05E-12	O	-2.01E-09
G	-1.09E-02	P	-1.74E-11
H	2.61E-06	Q	2.52E-14
I	1.10E-06	R	2.42E-16

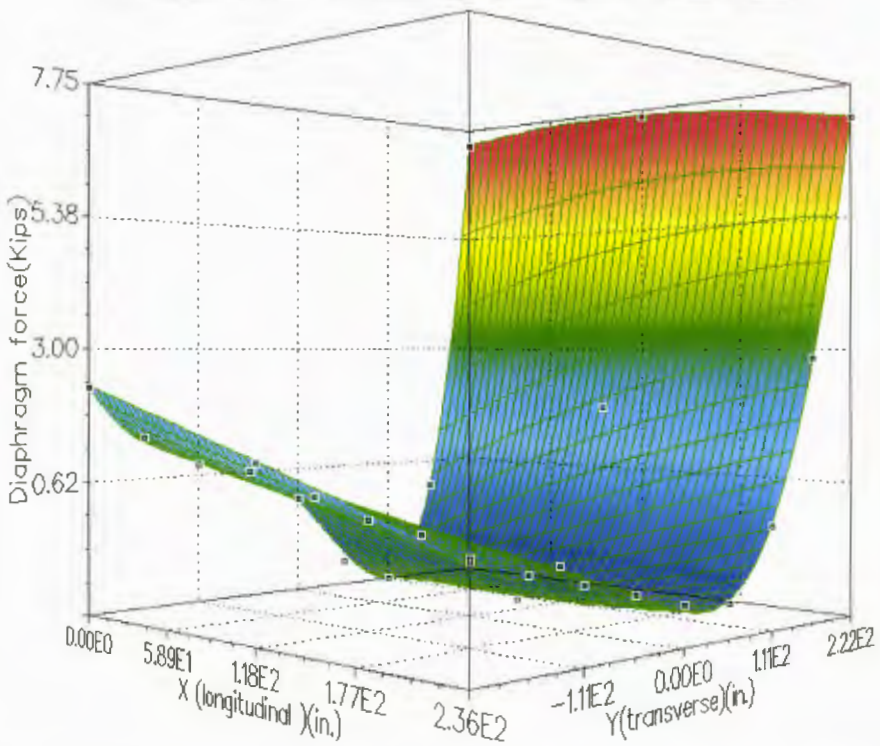

Fig.5.13 Three Dimensional Diaphragm Influence Surface Plot

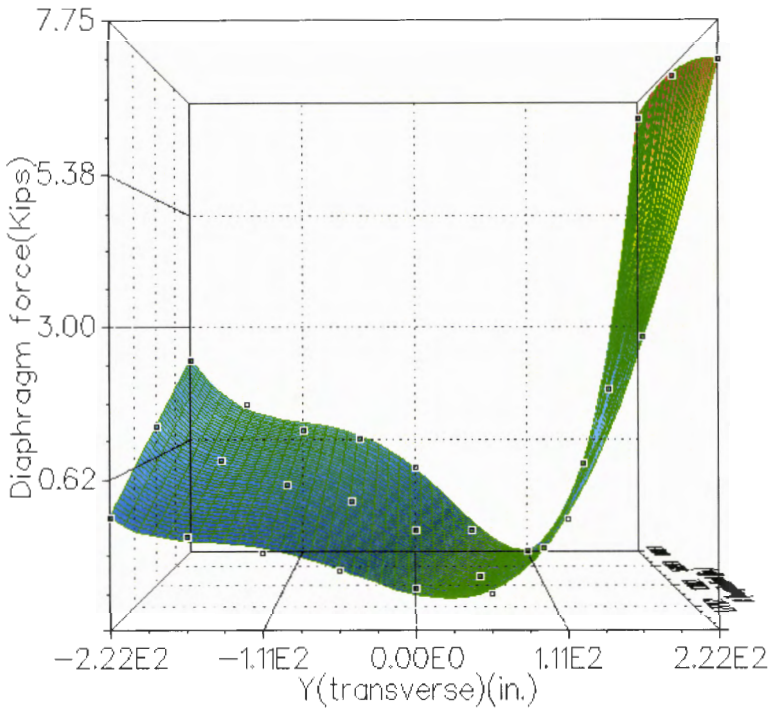

Fig.5.14 Front View of Diaphragm Influence Surface Plot

5.5.3 Influence surface for out-of-plane relative displacement of web-gap

Equation 5.1, with the vertical strain replaced by relative displacement, was used to predict the out-of-plane relative displacement in the web-gap region. In this case, the coefficients used in the equation given in Table 5.10., were used to represent the influence surface for out-of-plane relative displacement between the top and bottom critical nodes. Plots of the influence surface magnified by 100 are shown in Figs. 5.15 & 5.16.

Table 5.10 Coefficients of relative out-of-plane displacement influence equation

Coefficients		Coefficients	
A	-2.81E-07	J	3.01E-11
B	-6.07E-05	K	-3.76E-14
C	-1.71E-07	L	-4.55E-16
D	1.73E-09	M	2.03E-08
E	9.59E-12	N	1.85E-09
F	1.15E-15	O	-1.92E-12
G	-2.20E-05	P	-1.24E-13
H	-2.44E-07	Q	8.31E-18
I	2.19E-09	R	1.67E-18

To verify the accuracy of the equation of the influence surface for the relative out-of-plane displacement between the two critical nodes, comparison was made with the finite element results carried out with load case five positioned directly above the web-gap region. The top and bottom critical nodes gave -5.0862E-03 and 0.67968E-03in. out-of-plane displacements respectively which indicated a relative out-of-plane displacement value of 005765 in. The relative out-of-plane displacement predicted by Equation 5-1 was found to be 0.005836 in showing good agreement with the finite element results of load case five.

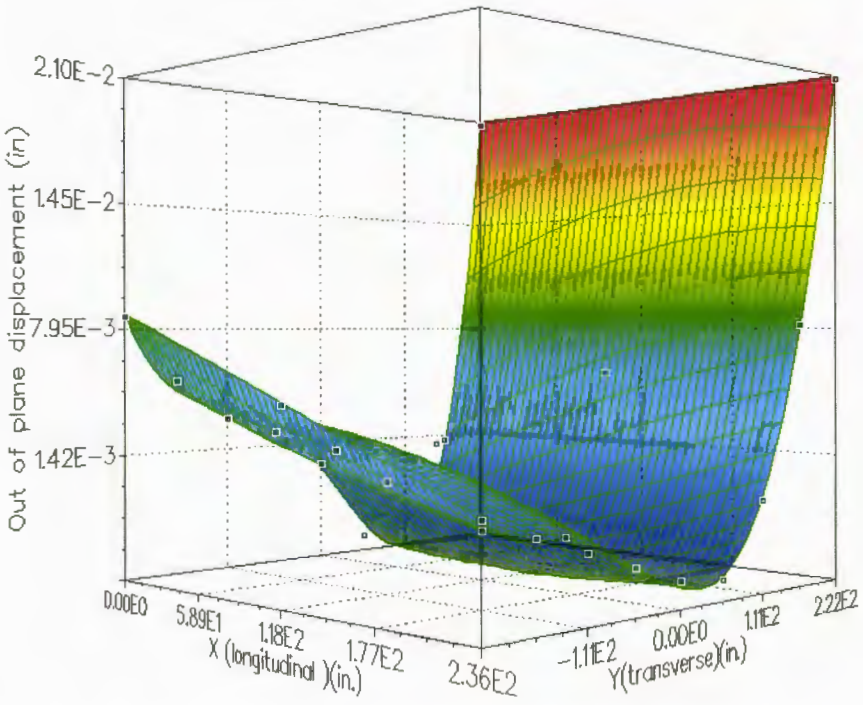

Fig.5.15 Three dimensional out-of-plane relative displacement influence surface between the critical nodes of the web-gap

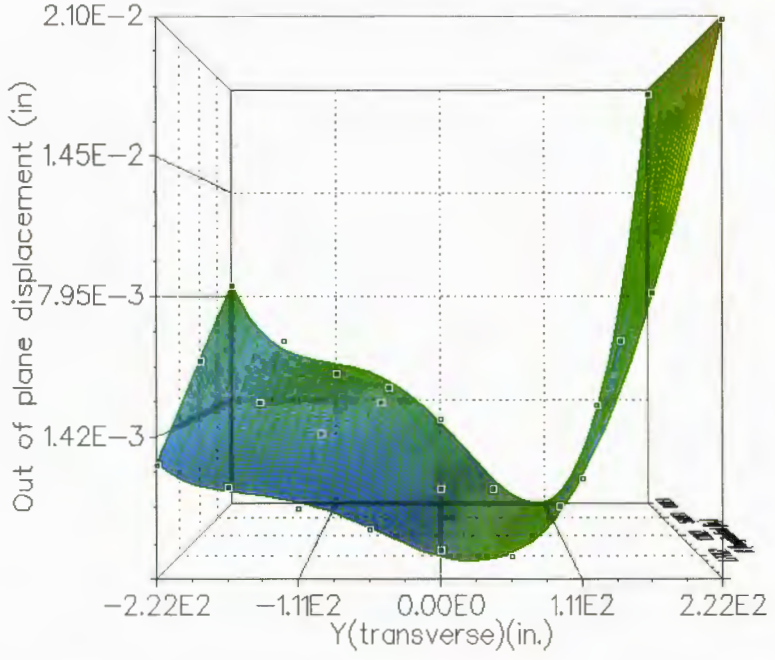

Fig.5.16 Front view of out-of-plane relative displacement influence surface between the critical nodes of the web-gap

It can be seen from the previous plots of the influence surfaces of the out-of-plane relative displacement, the diaphragm force and the strains in the web-gap that direct correlation exists among the three confirming that web-gap distortion is due to the force in the diaphragm induced by the differential deflections of girders.

5.6 Vertical stress verses relative out-of-plane displacement

The data that was utilized to derive the influence surfaces was also adopted to develop relationships between the vertical stresses and the relative out-of-plane displacements at the critical locations. In these relations, the relative out-of-plane displacement is defined as the difference between the displacements at the bottom and top critical points. The relative displacement is considered positive if the bottom critical point displaces away from the stiffener side. Figure 5.17 shows the linear relationships that were fitted for the stiffener and opposite to stiffener sides of the top and bottom critical locations.

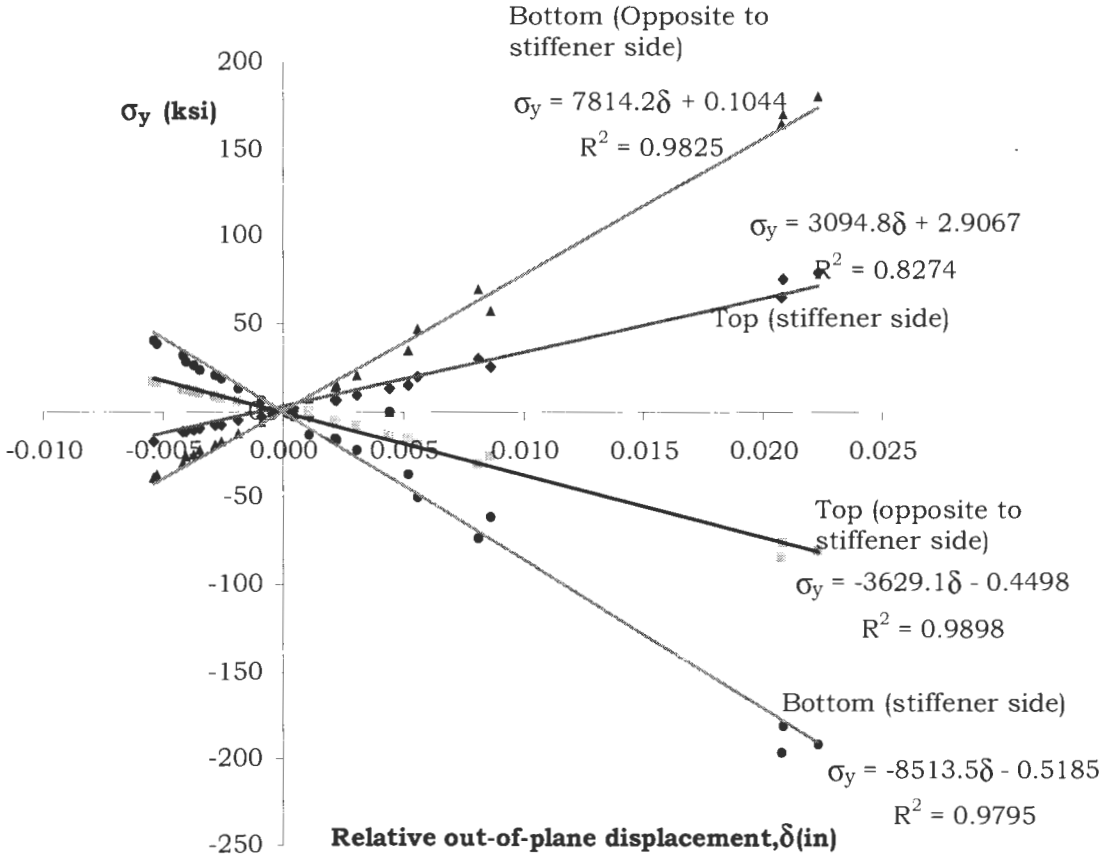

Figure 5.17 Vertical stress vs. relative out-of-plane displacement at critical locations

6. SUMMARY, CONCLUSIONS AND RECOMMENDATIONS

6.1 Summary

Crack formation due to out-of-plane distortion in the web-gap region has been a common occurrence in multi-girder steel bridges. The finite element method was adopted as an analysis tool to investigate the effects of different retrofit methods to minimize the out-of-plane distortion that results in the formation of these cracks. Three-dimensional finite element models for a continuous-skewed-steel-girder bridge were built using the ANSYS software. Coarse-models that included the two central spans of the bridge were built. The two spans modeled were sufficient enough to represent the distortion-induced in the web-gap region at the central pier since positioning truck loads on the two exterior spans was found to have insignificant impact on the distortion that was induced in the web-gap region. Sub-models for the web-gap region were next developed using finer mesh to obtain more accurate results.

The as-built bridge was retrofitted with a connection plate between the web-stiffener and top flange. Alternative retrofits, which included loosening of the bolts connecting the cross bracings to the web-stiffener, or adding an external stiffener on the opposite side of the web-stiffener, were considered. In addition, the web-gap with no provision of repair methods was utilized as a base line to evaluate the effectiveness of the various

retrofits alternatives as well as to study the impact of web-gap height on web-gap distortion. All these necessitated the development of a total of four coarse-models and six sub-models for the specific purposes under consideration.

The bridge structure was tested considering eight load cases. The induced strains and the out-of-plane displacements in the vicinity of the web-gap region were recorded. Verification of the finite element model developed was done by comparing the analytical strains with the corresponding strain results from the field tests that were measured in the web-gap region. The comparison was carried out using the load cases that were believed to be critical, i.e., the load cases that would induce significant differential deflections between the exterior and adjacent girders.

Influence surfaces for the strains, out-of-plane displacements at various locations, including the critical spots of the web-gap region were developed. In addition, influence surfaces were also constructed to estimate the forces in the cross bracing member. These were developed utilizing the results obtained from the numerous analyses of the bridge structure under a unit load that was poisoned and different locations.

6.2 Conclusions

The following are the conclusions that were attained based on the field test and the analytical study presented herein:

- The comparison of the results of finite element analysis with the field test results showed some discrepancy, especially for the load positioned directly above the web-gap. This discrepancy resulted from not being able to position the load exactly above the web-gap.
- Better agreement between the comparisons of the field and finite element analysis results was observed in the case of positioning of the load away from the web-gap region and for the bottom strain-gage locations.
- The as-built retrofit of the bridge with the provision of a plate connecting the web-stiffener with the top flange of the girder was found to have effectively reduced the out-of-plane distortion that would have been induced in the web-gap.
- The full bolt-loosening retrofit alternative resulted was found to significantly lower the strains and stresses induced in the web-gap.
- The addition of an external stiffener to the web-gap reduced the out-of-plane distortion in the region but was not as effective as the other retrofit methods considered.
- The height of the web gab has some effects on the stresses and strains that are induced in this region. The results showed that the short

web-gap height resulted in the highest vertical and principal strains induced in the web-gap region.

- The developed influence surfaces for strains, relative out-of-plane displacement and diaphragm force are instrumental to provide quick estimate of the effect of truck load positioning on the responses (strains, out-of-plane displacements and diaphragm forces and to investigate the distortion that takes place in the web-gap region.
- The correlation between diaphragm force, out-of-plane displacement and strain induced in the web-gap from the equations of the influence surfaces of these responses confirmed that the differential deflection between girders had been the cause of web-gap distortion.
- For the bridge under study a quick estimate of the vertical stress at the critical locations in the web-gap region can be achieved combining measurements of out-of-plane displacements by transducers and the developed linear stress-displacement relationships.

6.3 Recommendations

The following recommendations are suggested for future research:

- Due to the sensitive nature of the web-gap region, strain-gages should be placed at the critical locations of the maximum strains. Strain rosettes would be more accurate so that one can calculate the range of the principal strains at these critical locations.
- One must carefully monitor the positions of the truck on the bridge deck and record corresponding strain readings during field tests. This is important, especially if the results of these tests are used as a basis for calibration of finite element analysis results.
- Fatigue life of the web-gap region needs to be studied. This can be accomplished utilizing the influence surfaces in this work.
- Influence surfaces for strains and stresses in the web-gap region in bridges with different diaphragm types need to be developed. This would be an invaluable alternative to study effect of the out-of-plane distortion without the need of utilizing complex finite element analysis.

BIBLIOGRAPHY

1. AASHTO. (1992).*Standard Specifications for Highway Bridges, 15th Edition*, American Association of State Highway and Transportation Officials, Washington, D.C.

2. ANSYS (2002). *ANSYS Release 6.1*, ANSYS, Inc., Canonsburg, Pa.

3. Jajich, D., and Schultz, A.E. (2003). "Measurement and Analysis of Distortion-Induced Fatigue in Multigirder Steel Bridges." *Journal of Bridge Engineering*, 8(2), 84-91.

4. Khalil, A. (1998). *Aspects in Nondestructive Evaluation of Steel Plate Girder Bridges*, Dissertation., Iowa State University, Ames, Iowa.

5. Roddis, W. M. K., and Zhao, Y. (2001). "Out-of-plane fatigue cracking in welded steel bridges: Why it happened and how it can be repaired." *Welding innovation*, 27(2), 2-7.

6. Roddis, W. M. K., and Zhao, Y (2003). "Finite-Element Analysis of Steel Bridge Distortion-Induced Fatigue." *Journal of Bridge Engineering*, 8(5), 259-266.

7. Roddis, W. M. K., and Zhao, Y (2003). "Finite Element Study of Distortion-Induced Fatigue in Welded Steel Bridges." *Transportation Research Record 1845*, Transportation Research Board, National Research Council, Washington, D.C., 57-65.

8. Wipf, T. J., Greimann, L.F., and Khalil, A. (1998). *Preventing Cracking at Diaphragm/Plate Girder Connections in Steel Bridges*, Iowa State University, Ames, Iowa.

9. Wipf, T. J., Greimann, L.F, Wood, D. L., Phares, B. M., and Tarries, D. (2003). *Retrofit Methods for Distortion Cracking Problems in Plate Girder Bridges*, Center for Transportation Research and Education, Iowa State University, Ames, Iowa.